Optimizing Cardiac MR Imaging: Practical Remedies for Artifacts[1]

Farhood Saremi, MD • John D. Grizzard, MD • Raymond J. Kim, MD

TEACHING POINTS
See last page

With ongoing technical advances in magnetic resonance (MR) imaging, the clinical demand for cardiac MR evaluations has been increasing. Cardiac MR imaging techniques have evolved from traditional spin-echo sequences to breath-hold spoiled gradient-echo and balanced steady-state free precession sequences. The most recently developed techniques allow evaluation of myocardial function, perfusion, and viability; coronary angiography; flow quantification; and standard morphologic assessments. However, even with the most sophisticated acquisition techniques, artifacts commonly occur at cardiac MR imaging. Knowledge of the origin, imaging appearance, and significance of these artifacts is essential to avoid misinterpreting them as true lesions. Some artifacts are caused by simple errors in positioning of the patient, coil, or electrocardiographic leads; radiofrequency interference from nearby electronic equipment; or metallic objects within the magnetic field. Others are directly related to a specific MR imaging sequence or technique. Accelerated imaging techniques such as parallel imaging, which are used to shorten acquisition and breath-hold times in cardiac evaluations, are particularly vulnerable to artifacts. If an artifact severely degrades image quality, the acquisition should be repeated with appropriate adjustments to decrease or eliminate the problem.

©RSNA, 2008 • *radiographics.rsnajnls.org*

Introduction

With recent technologic advances in magnetic resonance (MR) imaging hardware and software, many techniques now are available for cardiac MR imaging. Recently developed techniques have expanded the clinical applications for cardiac MR imaging to include assessments of myocardial function, perfusion, and viability; flow quantification; and coronary angiography (1–9). Good image quality is the primary requisite for accurate interpretation of cardiac MR images. However, even if images are obtained by well-trained staff using sophisticated techniques, it is impossible to eliminate every artifact from MR images. In addition to ghosting, geometric distortion, and ripple artifacts, which are familiar to radiologists who regularly perform MR imaging, many other kinds of artifacts may occur at cardiac MR imaging that are specific to the modality or the acquisition technique (Table). Moreover, new types of artifacts emerge regularly as new imaging techniques are developed (10). To avoid misinterpreting an artifact as a true lesion, it is essential to be familiar with the various artifacts that may appear at cardiac MR imaging and to understand their effects on the quality of imaging data. In the case of severe artifacts, it is also important to know how to avoid or minimize the problem. The article provides an overview of artifacts that may be seen in cardiac MR imaging and offers practical remedies for eliminating or mitigating them.

Patient Preparation and Positioning

Various measures may be taken before or during image acquisition to avoid or mitigate artifacts. First, the importance of breath holding should be explained to the patient before the imaging examination. Image acquisition at end expiration is preferred because it is more reproducible (11).

Second, because almost all cardiac sequences are gated to the patient's cardiac cycle, electrocardiographic (ECG) leads should be applied and the ECG waveform evaluated before image acquisition is begun. A tracing that has poor amplitude requires lead repositioning. However, even with optimal lead placement, magnetohydrodynamic effects from flowing ions in the magnetic field (especially at high field strengths such as 3.0 T) and gradient switching noise may degrade tracings after the patient is placed within

---

Classification of Cardiac MR Imaging Artifacts according to Cause

Nonspecific MR imaging–related artifacts
  Inadequate SNR due to positioning errors
    Patient not positioned at center of magnet
    Surface coil not centered around heart
  Cardiac ghost due to malpositioned ECG electrodes
  Ghosts of heart and chest wall due to faulty breath hold
  RF interference from electronic devices (monitoring devices, drip stands, injection systems) near the magnet
Artifacts specific to cardiac imaging sequences and parameters
  Cine (functional) imaging: flow- and cardiac gating–related artifacts, bands
  Parallel imaging: aliasing artifacts and increased image noise
  First-pass contrast-enhanced (perfusion) imaging: dark rim (truncation, magnetic susceptibility) and aliasing artifacts
  Delayed contrast-enhanced (viability) imaging: effects of incorrect TI, suboptimal delay at contrast-enhanced imaging, B_1 field inhomogeneity, motion, poor ECG gating, long T1 species, short T1 in fat, and volume averaging
  Phase contrast imaging: aliasing artifacts caused by inappropriate maximum velocity settings, imaging plane malalignment, and partial-volume averaging
  Dark-blood (morphologic) imaging: artifacts related to suboptimal timing of data acquisition
Artifacts caused by ferromagnetic materials inside or on the patient (embedded foreign objects, prosthetic cardiac valves, external pacemaker wires, surgical wires and clips)

Note.—ECG=electrocardiographic, RF=radiofrequency, SNR=signal-to-noise ratio, TI=inversion time.

---

the magnet. The use of vectorcardiography may help improve the quality of gating (12).

Third, the placement of surface coils in relation to the heart is very important. The preferred coils for cardiac imaging are dedicated cardiac coils and dedicated torso array coils. In order to achieve a good signal-to-noise ratio (SNR), the center of both the anterior and the posterior surface coils should be well aligned with the center of the heart (Fig 1). Furthermore, since the homogeneity of the magnetic field decreases with increasing distance from the magnet isocen-
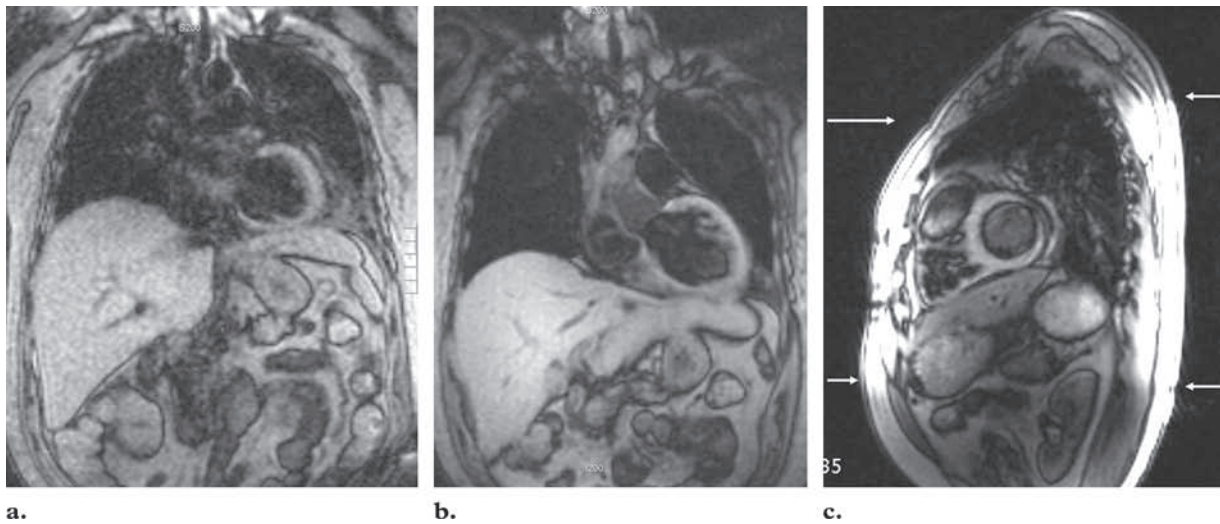
Figure 1.   Importance of patient and coil positioning. **(a)** Coronal scout image, acquired with the anterior coil array centered too low over the cardiac region and the heart positioned too far from the isocenter of the magnet, has an insufficient SNR. **(b)** Coronal scout image, acquired after repositioning of the anterior coil array over the heart and repositioning of the patient with the heart at the magnet isocenter, shows a significant improvement in the SNR. **(c)** Sagittal scout image obtained for verification of the coil position shows correct centering of the surface coils around the cardiac region (arrows).
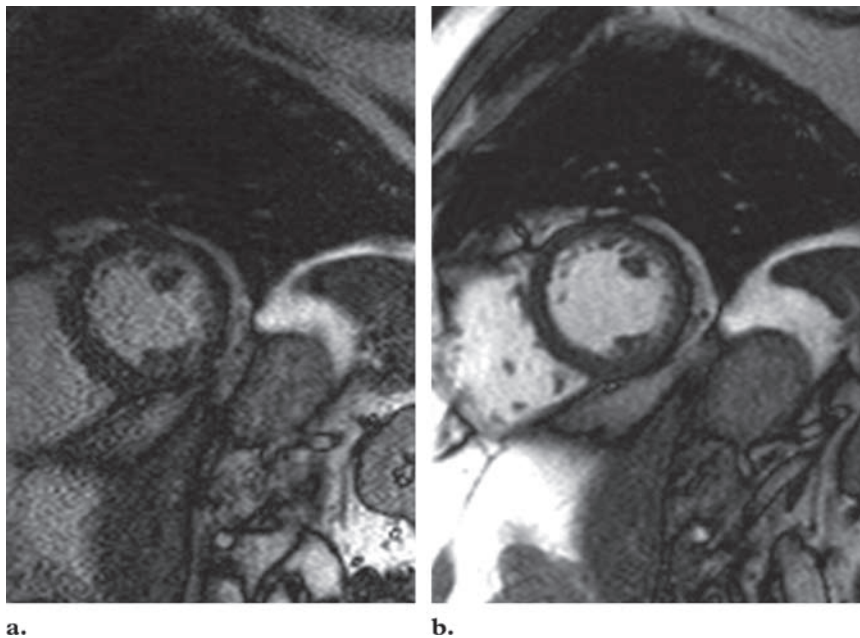

Figure 2.   Importance of activating both anterior and posterior coil arrays. Short-axis balanced steady-state free precession (SSFP) cine images acquired without **(a)** and with **(b)** activation of the anterior coil array demonstrate a marked loss of SNR in **a** compared with that in **b**.

ter, the center of the imaging volume should be placed at the isocenter.

After the patient is positioned within the magnet, multiplanar scout images should be obtained and reviewed to ensure that the surface coils are properly positioned over the heart and that the patient is positioned so that the heart is at or near the magnet isocenter. Sagittal images are the most useful for verifying the surface coil position (Fig 1c). It is also important to recheck all coil power connections before beginning the image acquisition. Excessive noise on an image could be due to the unintended disconnection of a coil from the power source (Fig 2).
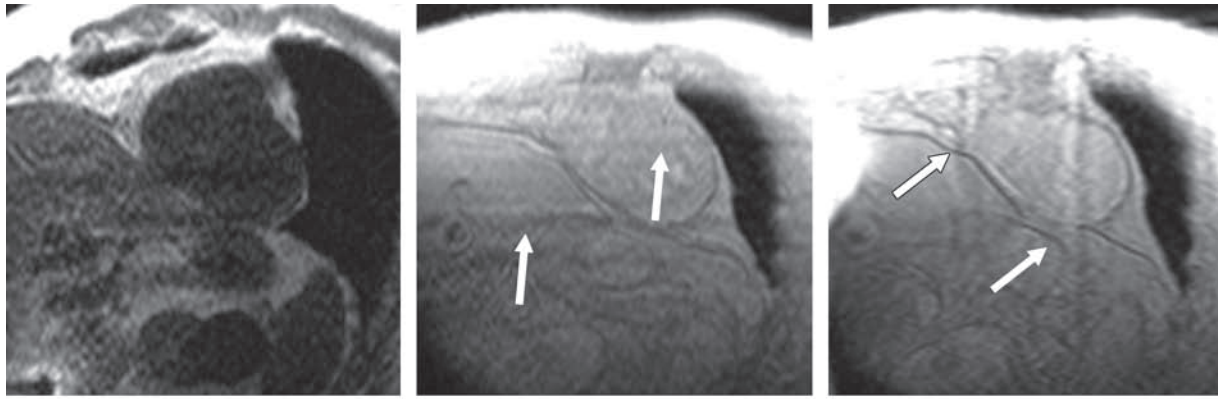
3a.   3b.   3c.

Figures 3, 4. General MR imaging artifacts. **(3)** RF artifacts produced by interference from an electronic monitoring device in the imaging suite. **(a)** MR perfusion image from a trial acquisition shows straight line artifacts in the phase-encoding direction (horizontal axis). **(b)** Perfusion image obtained without the preparatory pulse shows a marked decrease in the severity of the artifacts (arrows). **(c)** Perfusion image obtained by exchanging the frequency- and phase-encoding directions shows a shift in orientation of the artifacts (arrows) from the horizontal to the vertical axis. **(4)** Spike artifact. MR perfusion image shows a pattern of regularly spaced lines produced by corrupt data points in k-space. The frequency and orientation of the lines depend on which k-space points are affected.

4.
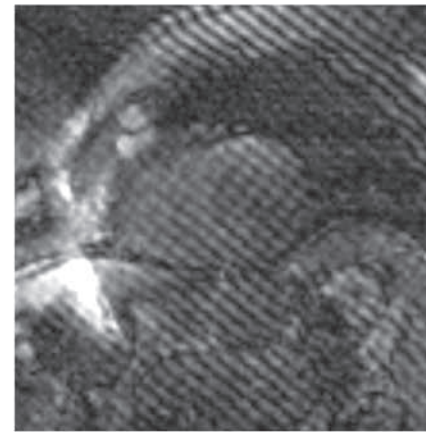
General MR Imaging Artifacts

Radiofrequency (RF) artifacts are straight lines that extend across the image in the phase-encoding direction. These artifacts result from the interference of ambient RF waves with the MR signal. Such interference may occur because of incomplete closure of the door to the MR imaging suite or inadequate shielding of electronic devices used for patient monitoring or contrast material injection (10).

Other sources of linear artifacts are stimulated echoes (which produce zipperlike lines) and spikes in k-space (which produce regularly spaced lines). Spike artifacts are caused by corrupted data points in k-space, which are due to instability of the magnet or to a breakdown of interconnections in the RF coil, not to RF contamination; these artifacts are more pronounced on images acquired with a high-frequency duty cycle (13,14). Whereas RF artifacts may be superimposed on all the images within a series from a single acquisition, spike artifacts are sporadic and usually transient (ie, limited to one or two images in a series) (Figs 3, 4).

Artifacts Specific to Cardiac Imaging

Cine Imaging

Two cine MR imaging techniques are commonly used to assess cardiac function: the segmented-k-space spoiled gradient-echo (GRE) sequence (4) and the balanced SSFP sequence (5). Balanced SSFP sequences provide better SNR, increased contrast between myocardium and blood, and, thus, greatly improved image quality in comparison with those obtainable with spoiled GRE sequences (5). Image acquisition with spoiled GRE sequences takes less time than that with balanced SSFP sequences applied at the same bandwidth; however, to achieve a good SNR at spoiled GRE imaging, a lower-frequency bandwidth typically is needed. Therefore, SSFP acquisitions may take less time than spoiled GRE acquisitions when standard settings are used.

In segmented approaches to image data acquisition, only a fraction of the total number of k-space lines is acquired during one heartbeat.
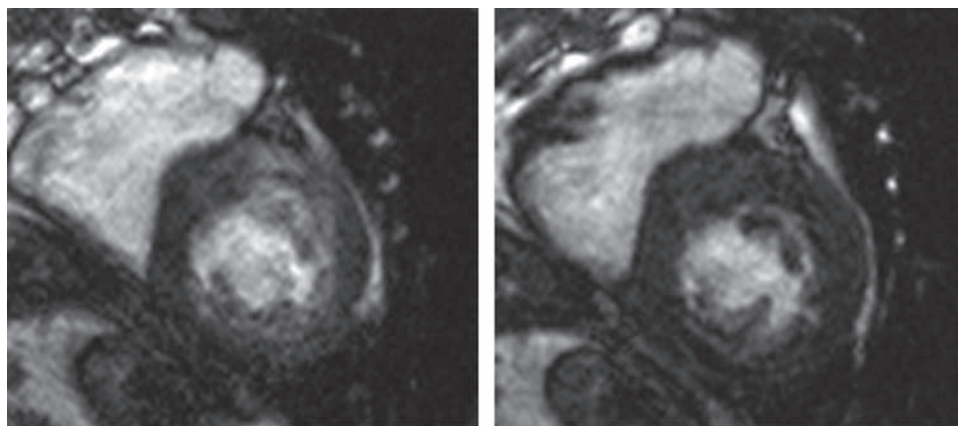
a.   b.

Figure 5. Cine cardiac MR images obtained with retrospective **(a)** and prospective **(b)** gating in a patient with atrial fibrillation and an irregular heartbeat show improved image quality in **b**, an image reconstructed from a data set that omitted end-diastolic information.

Typically, a breath hold that lasts 10–12 cardiac cycles is required to obtain all the k-space lines needed to fill the image matrix. Because of variations in the cardiac cycle over time, ECG gating is necessary.

In retrospective gating, which is the most commonly used method, the data for a given section are acquired continuously throughout the cardiac cycle and are time-stamped to allow their assignment to the proper segment of the cycle. Data from several different cardiac cycles are combined to yield a single cine sequence. Because a single acquisition spans multiple heartbeats, all segments of the cardiac cycle are included. However, the patient's heart rate and rhythm must be regular to produce high-quality images; irregularities in the cardiac cycle cause cine images to appear blurred. Most vendors incorporate arrhythmia rejection in their cine sequences, often by excluding cycles in which the R-R interval differs from a preset range of acceptable values. However, this method requires increased acquisition and breath-hold time, and therefore it is an imperfect solution. In patients with highly variable R-R intervals, prospective gating may be necessary.

In prospective gating, the onset of the R wave triggers the image data acquisition. To compensate for physiologic variations in heart rate, the acquisition window is usually 10%–20% shorter than the average R-R interval. Unfortunately, this means that the end of the cardiac cycle (late diastole, which often includes atrial contraction) is excluded from the image acquisition; thus, this method is not the first choice for evaluating diastolic function (including valvular flow), although it is suitable for use in evaluating systolic function. One potential advantage of prospective gating over retrospective gating is that it is less sensitive to variations in the duration of diastole such as those seen in patients with sinus arrhythmia and in some with atrial fibrillation (Fig 5).

In patients who cannot hold their breath for the duration of a segmented acquisition or in whom the ECG signal is weak, a single-shot technique may be used. With recent developments in gradient hardware, a repetition time (TR) of less than 3 msec is achievable with balanced SSFP MR imaging. The balanced SSFP sequence is now preferred for real-time functional imaging because it provides a high SNR even with a short TR (15,16). One entire cardiac cycle (one R-R interval), in one section location, is acquired at a time. The number of phases acquired per cardiac cycle depends on the heart rate and the usual tradeoff between spatial and temporal resolution. Although gating is not necessary for real-time imaging, when possible, prospective gating often is used to allow the synchronization of cine images from multiple section locations for viewing as movie clips (15). Real-time imaging may be
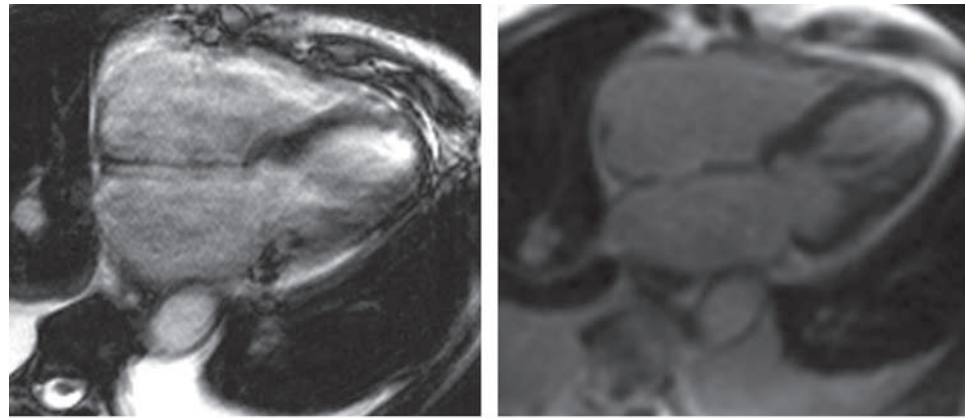
Figure 6.   Long-axis cardiac MR images acquired in the same 6-mm-thick section during the same phase of the cardiac cycle with different balanced SSFP sequences. **(a)** Image obtained with a standard breath-hold segmented balanced SSFP technique shows a marked artifact and an indistinct border between the myocardium and the left ventricular cavity because of breathing during image acquisition. **(b)** Image obtained with a real-time balanced SSFP parallel acquisition technique (time-domain SENSE) with prospective gating shows the elimination of the motion-related artifact. The endocardial contour is blurred, mainly because of a larger pixel size and poorer temporal resolution. Contrast between myocardium and blood also is inferior to that in **a** because of the larger pixel size and lower flip angle.

especially useful in patients with arrhythmia or reduced breath-holding capabilities. The disadvantage of real-time imaging in comparison with segmented acquisitions is a reduction in both spatial and temporal resolution (Fig 6). The reduced temporal resolution leads to a slight overestimation of end-systolic volume (16), which in turn may lead to underestimations of the stroke volume and ejection fraction. Parallel acquisition techniques may help improve the temporal resolution of real-time balanced SSFP cine acquisitions (17). In addition, radial or spiral rather than rectilinear sampling of k-space may be advantageous for increasing spatial resolution, temporal resolution, or both and for reducing artifacts (18).

Balanced SSFP (vendor-specific variants include TrueFISP, balanced FFE, and FIESTA) is a GRE sequence in which a train of RF excitation pulses with an alternating large flip angle (eg, ±60°) is used. All three gradient axes are fully balanced to produce steady-state magnetization. The signal intensity in balanced SSFP sequences depends on the T2/T1 ratio, which is high for blood and low for myocardium; the result is greater contrast between blood and myocardium than that attainable with spoiled GRE sequences (5).

Balanced SSFP imaging is useful for evaluating the cardiac anatomy and function but has limited value for tissue characterization based on signal intensity. A typical feature of balanced SSFP sequences is the very high signal intensities of both fluid and fat, which have completely different T1 and T2 values but similar T2/T1 ratios. Blood inflow or motion effects may further modify the contrast obtained with balanced SSFP sequences (19).

Balanced SSFP sequences initially had only limited application because of the high prevalence of banding artifacts on the resultant images. Banding (or dark band) artifacts are caused by the dephasing of spins with resultant loss of the steady-state signal during a single TR (19–24). These artifacts appear predominantly at off-resonance points in the magnetic field (Fig 7a) or wherever there is a significant disruption of field homogeneity. Therefore, banding artifacts are worsened by *(a)* a longer TR, *(b)* an off-resonance RF pulse (which occurs when the frequency of the RF synthesizer on the MR imaging system is different from the local precession frequency of magnetization), and *(c)* a significant field inhomogeneity.

On balanced SSFP images, the dark stripelike bands generally appear in stationary tissues at the edges of the field of view (FOV), where the
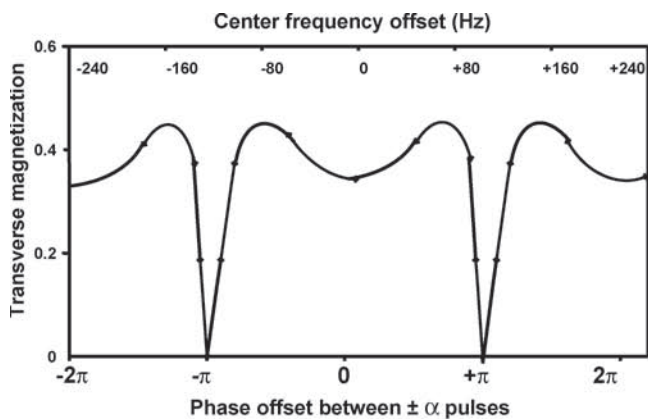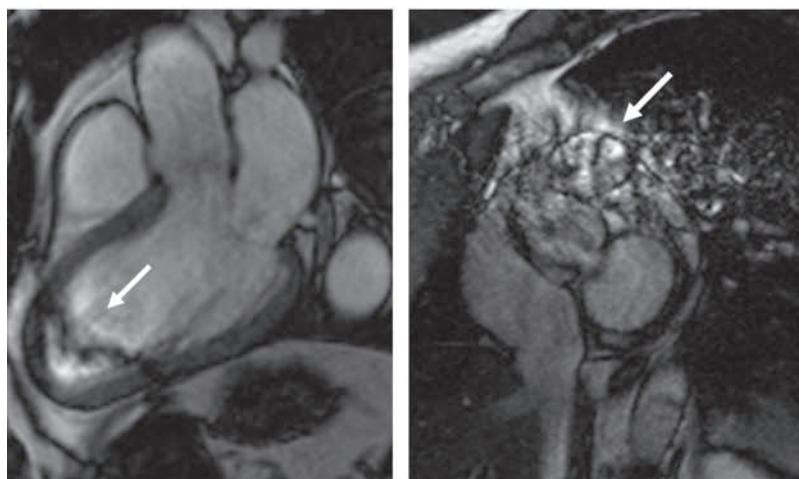
a.
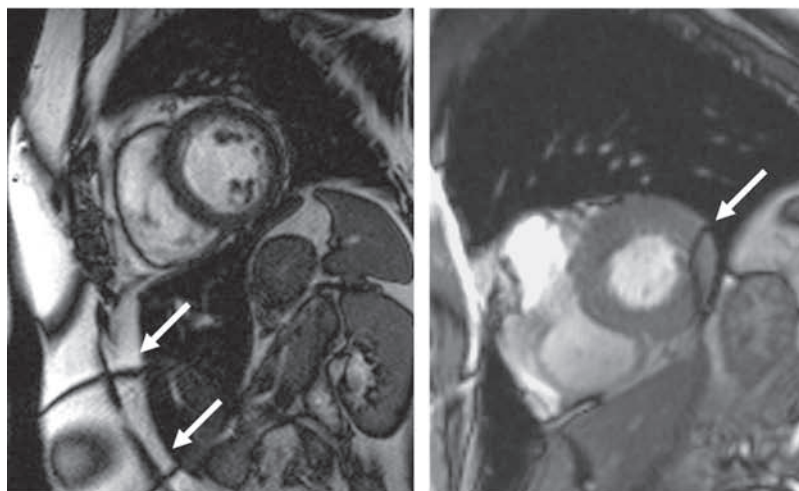
b.

c.

d.

e.

Figure 7. **(a)** Graph shows the steady-state signal amplitude achieved with a balanced SSFP sequence as a function of dephasing between pulses. The signal profile may be described as a plateau that is interrupted regularly by sharp decreases in amplitude near odd multiples of π radians or when the center frequency offset is larger. These off-resonance points produce dark band artifacts like those shown on the short-axis breath-hold SSFP cine images in **b–e**. **(b, c)** Dark band artifacts (arrows) are obvious in the high-signal-intensity stationary tissues near the edge of the FOV in **b** and in the inferolateral wall of the left ventricle in **c**. Such artifacts are less commonly seen in the lung and myocardium because those tissues have low signal intensity on SSFP images. **(d)** In another patient, a dark band flow artifact in the left ventricular cavity (arrow) has an irregular appearance because of the forward motion of the in-plane flow. **(e)** Image at the base of the heart in a third patient shows severe flow-related artifacts (arrow) caused by spins moving out of the plane of imaging near the position of a dark band artifact.

magnetic field is least uniform (Fig 7b). Such artifacts may not be visible in the myocardium and lungs because these tissues have low signal intensity on balanced SSFP images; the artifacts tend to be seen more often in high-signal-intensity areas (eg, blood and fat). However, they also may appear along the inferolateral wall of the left
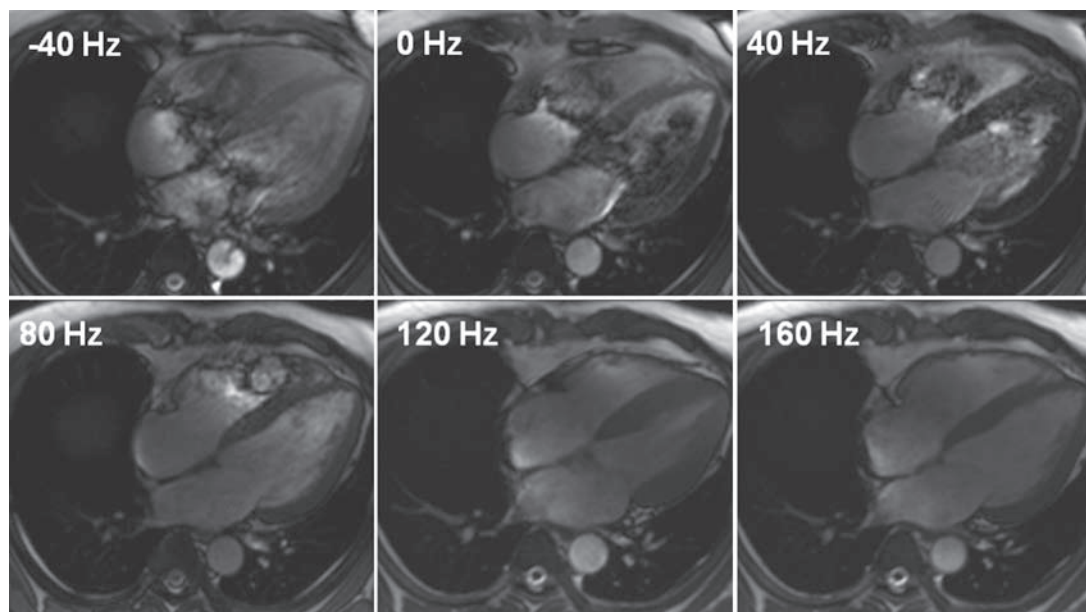
Figure 8. Frequency-shift technique. Balanced SSFP scout image series obtained with a 3.0-T magnet and with progressive increases in frequency (from −40 Hz to 160 Hz) shows gradual shifts in the position of a dark band flow artifact across the heart until the left ventricle is unobstructed.

heart structures (21) (Fig 7c). When a dark band artifact appears in flowing blood, its form fluctuates with the flow profile, resembling a pulsating fluid jet or giving the impression of being dragged along with the flow (Fig 7d). In regions with fast-flowing blood (eg, at the base of the heart or the aorta), spins flowing out of the imaging plane also may cause severe artifacts (Fig 7e).

Because dark band artifacts are related to inhomogeneities in the magnetic field or center frequency offsets, they may be substantially reduced by reshimming and retuning of the imaging system. This may be accomplished by performing the following steps: First, the TR must be minimized. Reduced TR is achievable primarily by using improved gradient hardware. Increasing the bandwidth may allow a reduction in TR, but that reduction comes at the expense of a reduction in SNR. Other methods to decrease the TR include asymmetric readout as well as reduced spatial resolution. Second, since the ability to minimize TR is limited by the specific absorption rate (particularly at 3.0 T), increased attention must be given to shimming to maximize the main field homogeneity. A volume shim centered on the left

ventricle works best. During shimming, it is helpful to ask the patient to breathe shallowly so as to minimize chest motion. Third, if dark band artifacts are not fully suppressed after shimming, the center frequency should be aligned more closely with the water resonance frequency. This can be done manually or by acquiring a frequency-shift scout image series (Fig 8). Adjusting the center frequency will cause the dark bands to shift in location (25).

Parallel Imaging

Fast imaging with high temporal and spatial resolution is of great importance in most cardiac MR imaging applications (26–28). Parallel imaging methods may help accelerate image acquisition, but at the costs of reduced SNR and increased artifacts. In general, the SNR is reduced by at least the square root of the acceleration factor. In its most common application at 1.5 T, an acceleration factor of two is used. An additional decrease in SNR may be expected, with the size of the decrease depending on the geometry factor of the underlying coil array (27).

Various reconstruction algorithms have been developed for parallel imaging, including simultaneous acquisition of spatial harmonics, or SMASH (26); sensitivity encoding (SENSE)

Teaching Point

Teaching Point
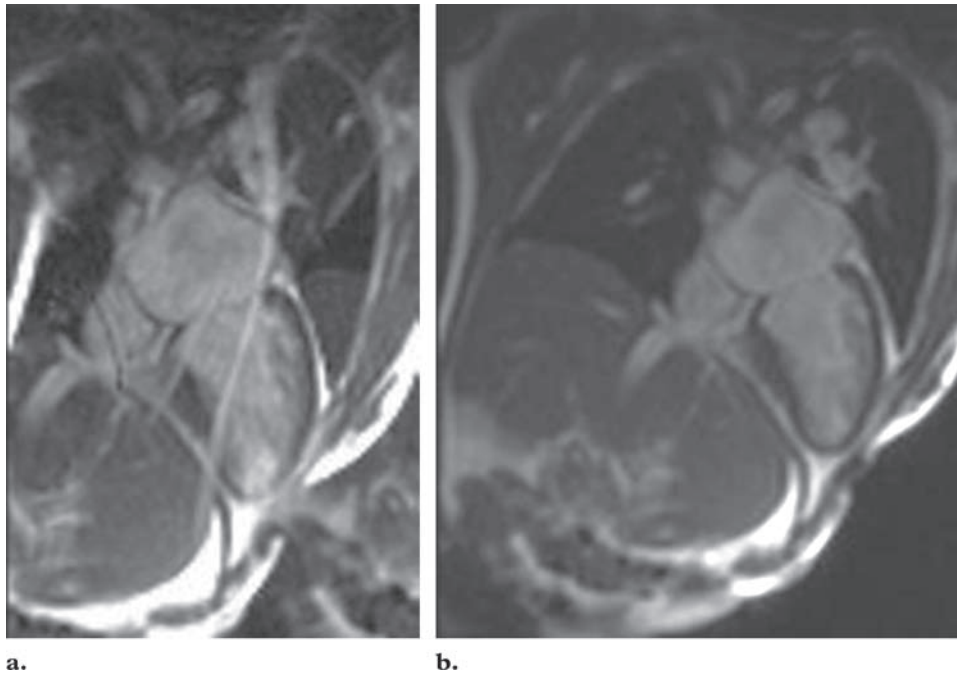
a.   b.

Figure 9. Real-time balanced SSFP cine cardiac images obtained with dynamic parallel imaging (SENSE), ECG triggering, and breath holding. **(a)** Image shows multiple aliasing artifacts (due to peripheral fat) at the center, the effects of too small an FOV (350 mm). **(b)** Image obtained with a larger FOV (400 mm) shows an absence of artifacts.

(27); and generalized autocalibrating partially parallel acquisition (GRAPPA) (28). In SENSE, the spatial sensitivity profile of each coil is used to separate the aliased signals pixel by pixel and reconstruct a single full-FOV image (image-based reconstruction). In GRAPPA, the spatial sensitivity data from each receiver coil are used to interpolate the acquired data to fill in the missing lines in k-space (k-space–based reconstruction). The SENSE technique requires a separate reference acquisition to allow the system to determine the spatial sensitivity profiles. By contrast, GRAPPA requires no reference acquisition because it is self-calibrating (auto-calibrating). A primary advantage of autocalibration is the ability to avoid the motion-related artifacts that may result from misalignment of the reference acquisition with the main acquisition in SENSE. However, the use of autocalibration reduces the effective acceleration factor of sequences such as GRAPPA. Other image-based parallel imaging techniques (besides GRAPPA) that provide autocalibration include the modified SENSE and generalized encoding matrix, or GEM, techniques (29,30).

Parallel imaging methods are currently proving useful in cardiac imaging at 3.0 T. At this higher magnetic field strength, the SNR is higher, but specific absorption rate limits are more likely to be exceeded (31–33). The use of parallel imaging

techniques decreases the RF deposition required to generate an image by an amount approximating the acceleration factor, while the strong signal at 3.0 T allows a substantial acceleration of image acquisition with maintenance of a sufficient SNR (31–33). However, these accelerated acquisitions are prone to artifacts.

A residual aliasing artifact specific to SENSE imaging has been described (34). The characteristic "wraparound" artifact occurs when the reconstructed FOV is smaller than the object imaged (Fig 9). SENSE imaging does not allow the "unwrapping" of the overlapped image data. Unlike the aliasing artifacts that occur at conventional (nonparallel) imaging, these artifacts appear not only at the edges of the FOV but also at its center. To remove these aliasing artifacts, the size of the FOV may be increased; however, this solution results in decreased spatial resolution. The number of phase-encoding steps also may be increased; this will reduce the effective acceleration factor while maintaining the same spatial resolution. The location of the SENSE artifact depends on the SENSE factor; the artifact moves closer to the edge of the image as the SENSE factor is reduced (34). GRAPPA offers an advantage over SENSE when the FOV is smaller than the
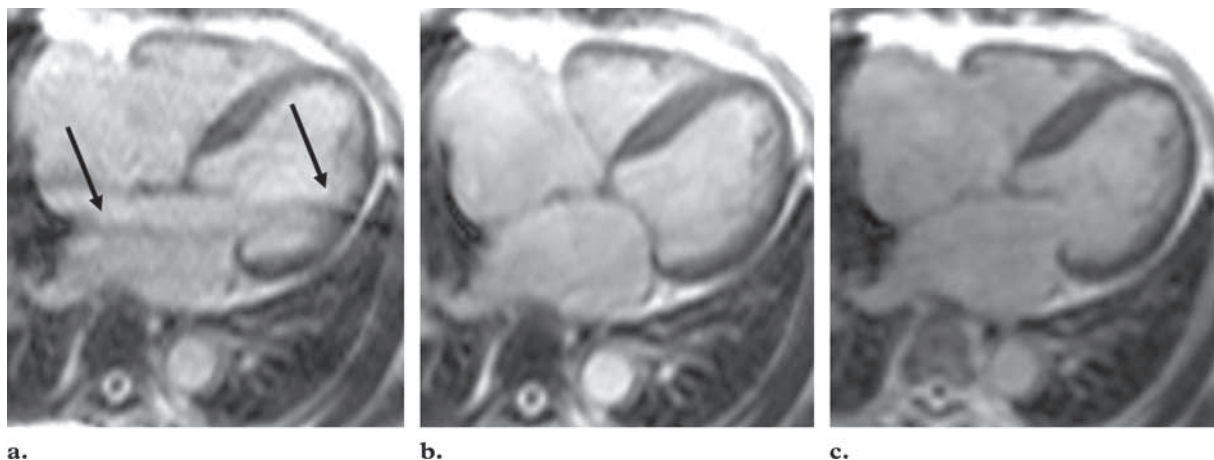
a.   b.   c.

Figure 10.   Real-time single-shot balanced SSFP images obtained with the same FOV (360 × 225 mm) but with three different reconstruction techniques. **(a, b)** Image obtained with GRAPPA **(a)** is degraded by aliasing artifacts and increased noise in comparison with that on the image obtained with the conventional reconstruction algorithm **(b)**. **(c)** Image obtained with time-domain SENSE shows a reasonable SNR and decreased artifacts when compared with **a**.

object imaged (especially in cardiac imaging) because it is relatively invulnerable to wraparound artifacts (29). However, SENSE produces a higher SNR than that achievable with GRAPPA; coil calibration errors may result from signal variations between the calibration and reconstruction processes in GRAPPA, causing the amplification of noise on images (Fig 10a). Methods for suppressing this amplified noise have been proposed (35).

The most recent advances in the field of parallel imaging are dynamic parallel acquisitions in the time domain with the use of a time-domain SENSE or time-domain GRAPPA sequence. These techniques help significantly improve the performance of cine and dynamic cardiovascular imaging while maintaining a sufficient SNR (36–38). Because these techniques incorporate a low-pass temporal filter, they are tolerant of coil and body motion and may help suppress residual aliasing artifacts due to errors in coil sensitivity estimates (Fig 10c).

Myocardial Perfusion Imaging

The goal of MR imaging of myocardial perfusion is to depict with high spatial and temporal resolution the first pass of intravenous contrast material through the myocardium (6–8,37). MR perfusion imaging is most commonly performed after the administration of a gadolinium-based contrast material (0.05–0.1 mmol gadolinium per kilogram of body weight) at a rate of 3–5 mL/sec, followed by a saline flush (30–40 mL) administered at the same rate.

The MR imaging techniques most commonly used for evaluation of myocardial perfusion are spoiled GRE sequences with or without the incorporation of hybrid echo-planar techniques to increase imaging speed (7,8). Short echo time (TE), short TR, and magnetization preparation pulses are commonly used to increase T1 contrast in the myocardial region. Standard magnetization preparation includes section-selective or non-selective 90° saturation-recovery pulses (8,39). Alternative techniques such as balanced SSFP sequences may help improve SNR at perfusion imaging (40,41). Three to five image sections may be acquired over 40–60 heartbeats, depending on the duration of the R-R interval. The temporal resolution for perfusion imaging is typically one cardiac cycle (R-R interval) or, in patients with tachycardia, every other R-R interval. Parallel imaging methods may be incorporated to further decrease the acquisition time (increase the number of sections acquired per R-R interval).

Although research studies often emphasize quantitative analysis, a simple visual assessment is the most common approach used to interpret first-pass perfusion images in the clinical setting.
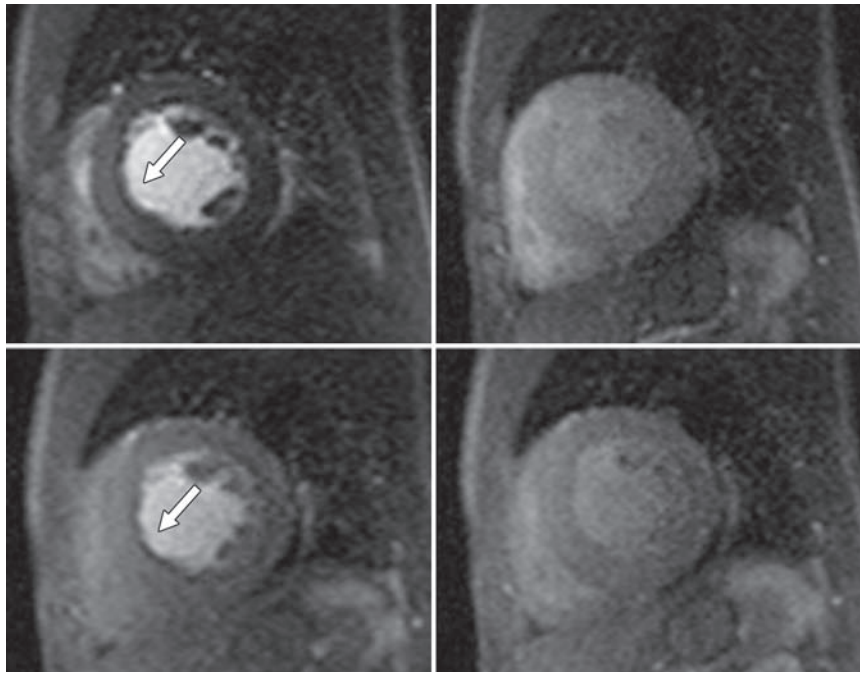
Figure 11. First-pass MR perfusion image series obtained with a saturation-recovery spoiled GRE sequence with parallel imaging (time-domain SENSE) during stress (top row) and rest (bottom row). Early views obtained as the contrast material arrived in the left ventricle (left column) show a dark rim artifact (arrow) perpendicular to the phase-encoding direction (horizontal axis) at the border of myocardium and blood. The artifact is absent from delayed views obtained during washout (right column).

A true perfusion defect associated with epicardial coronary stenosis or myocardial infarction appears as a nonenhancing dark zone during the myocardial phase of contrast medium transit. The defect persists through at least three heartbeats, extends into the myocardial muscle (ie, beyond the subendocardium-cavity interface), and is more conspicuous during stress than at rest.

Dark Rim Artifacts.—Dark subendocardial rim artifacts are common in perfusion studies and may be confused with myocardial perfusion defects. These artifacts typically appear as dark lines at the border of blood flow and myocardium (Fig 11). They tend to be most prominent at the blood-myocardium interface and to be oriented perpendicular to the direction with the lowest spatial resolution (typically, the phase-encoding direction). Their orientation changes with a change in the phase-encoding direction (42).

Factors that may contribute to the production of dark rim artifacts include partial-volume averaging, gadolinium-induced magnetic susceptibility, myocardial motion, and undersampling from low spatial resolution, either alone or in combination (42–44). Investigators in one study suggested that dark rim artifacts are actually truncation artifacts and may be largely due to limited spatial resolution rather than motion (39).

Regardless of their cause, the artifacts are ameliorated by higher spatial resolution. Parallel acquisition schemes are the most efficient way to improve both temporal and spatial resolution (45). The greater SNR available with 3.0-T magnets may help offset the loss in SNR that results from incorporating parallel acquisition techniques. In addition, lower concentrations of gadolinium may be used at 3.0 T, leading to less severe magnetic susceptibility effects (46,47).

Aliasing Artifacts.—Aliasing artifacts are common in first-pass perfusion imaging and may be especially pronounced when parallel imaging techniques are used. As mentioned earlier, care must be taken to select a sufficiently large FOV (Fig 12). Rotation of the imaging plane to match the patient's chest wall anatomy may allow the use of a smaller FOV without resultant aliasing effects. It is extremely important to instruct the patient about the breath holding procedure before image acquisition is begun. Breath holding is especially vital as the contrast medium transits the left ventricular myocardium.

Figure 12. Unenhanced perfusion images obtained with a saturation-recovery spoiled GRE sequence with time-domain SENSE show an inverse relation between the severity of aliasing artifacts and the size of the FOV. **(a, b)** Ghosts from aliasing are significantly reduced when the FOV is increased from 240 × 320 cm **(a)** to 316 × 380 cm **(b)**. **(c)** A further reduction in aliasing effects is achieved by exchanging the phase-encoding direction with the frequency-encoding direction.

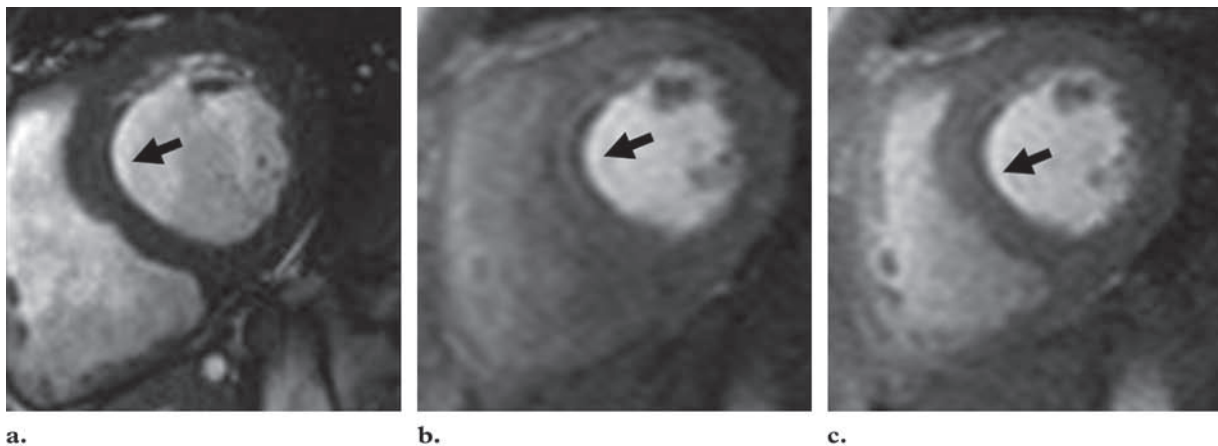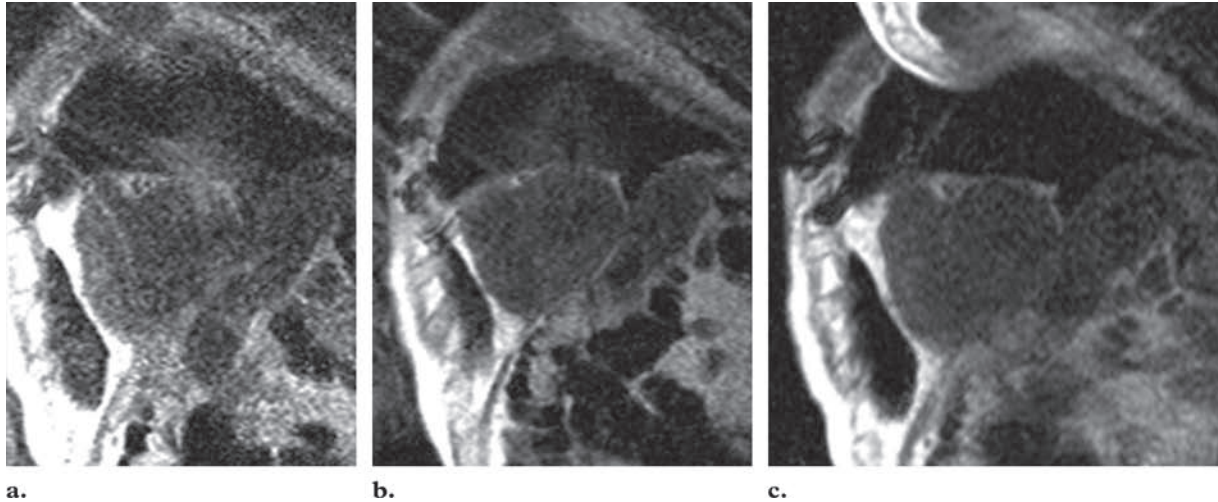a.   b.   c.

a.   b.   c.

Figure 13. Short-axis images obtained with a balanced SSFP cine acquisition **(a)**, saturation-recovery spoiled GRE perfusion acquisitions during stress **(b)** and rest **(c)**, and an inversion-recovery spoiled GRE acquisition **(d)** depict a subendocardial rim calcification with relatively low signal intensity (arrow) in the left side of the ventricular septum.

Calcifications and Thrombi.—Calcifications of the subendocardium and thin mural thrombi may be confused with perfusion defects resulting from ischemic heart disease. Calcifications are relatively easy to differentiate because they have low signal intensity on all perfusion images, including those acquired with balanced SSFP and GRE sequences (Fig 13). Thrombi have low signal intensity on perfusion images and viability images but may have signal isointense to that of myocardium on cine images.

d.

Delayed Contrast-enhanced (Viability) Imaging

The results of a number of studies have demonstrated the effectiveness of a segmented inversion-recovery spoiled GRE sequence for

Figure 14. **(a)** Inversion-recovery magnetization-time curves obtained with TI of 450 msec in normal myocardium (black line) and 250 msec in infarcted myocardium (gray line) show a null time of 312 msec—the TI at which longitudinal magnetization reached zero and the signal was nulled in normal myocardium. **(b)** Curves show signal intensities resulting from the application of an inversion preparatory pulse with various TI values in normal (black line) and infarcted (gray line) myocardium. Note that the signal intensity value corresponds to the magnitude of the magnetization vector and cannot be a negative number. **(c)** Curve shows the difference in signal intensity between infarcted and normal myocardium as a function of TI. The optimal TI is the point of maximum intensity difference. (Adapted, with permission, from reference 52.)
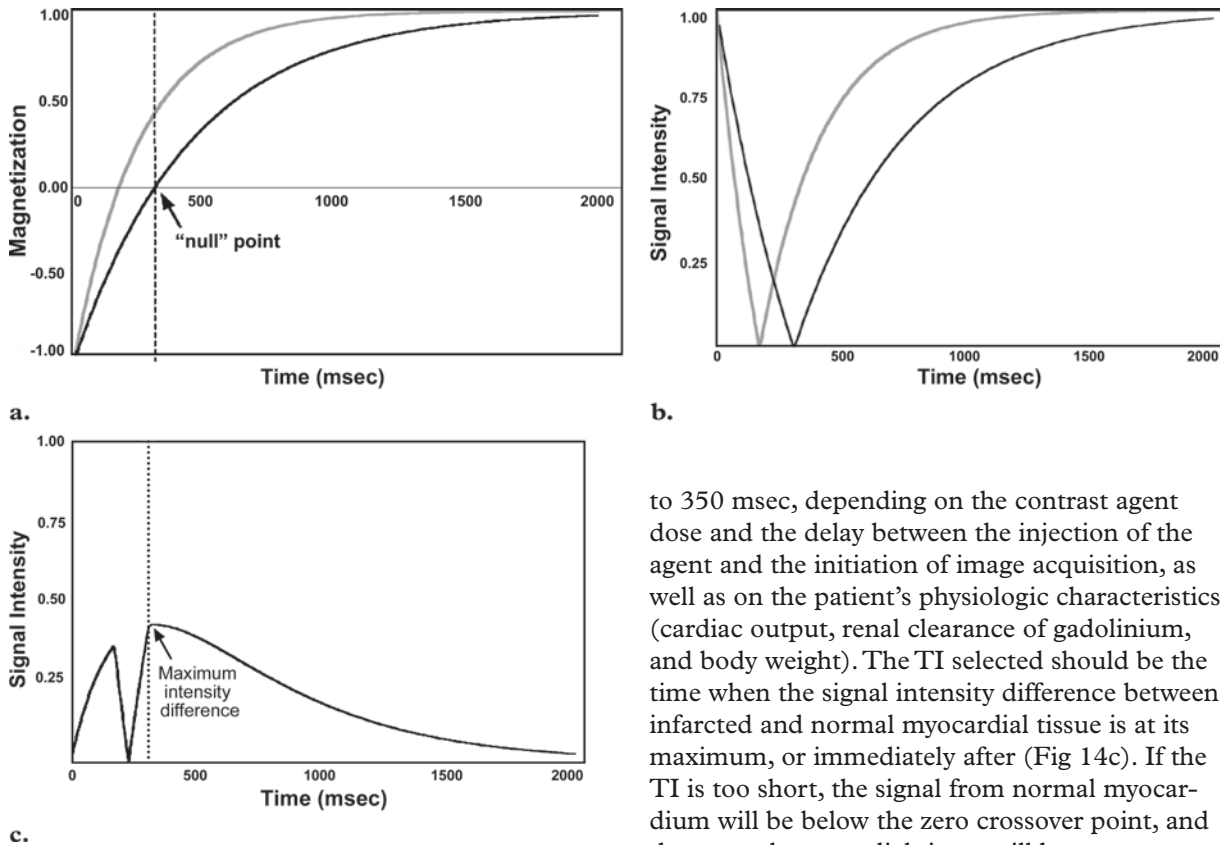
diagnosing the presence, location, and transmural extent of acute and chronic myocardial infarction (48–51). To minimize cardiac motion, image acquisition is performed in mid diastole by instituting a specified delay after the R wave on the ECG tracing. The magnetization of the heart is then prepared with a nonselective 180° inversion pulse to increase T1 weighting (51). The inversion time (TI) is defined as the time between this 180° pulse and the acquisition of the central lines (central k-space segment). With the segmented k-space approach, 23 lines of k-space are acquired in each data acquisition window, during every other heartbeat. Typically, a breath-hold duration of eight to 10 cardiac cycles is required to fill the image matrix.

Artifacts Due to Incorrect TI.—Selecting the appropriate TI is extremely important for obtaining accurate images (Fig 14). The TI to null the signal from normal myocardium varies from 200

to 350 msec, depending on the contrast agent dose and the delay between the injection of the agent and the initiation of image acquisition, as well as on the patient's physiologic characteristics (cardiac output, renal clearance of gadolinium, and body weight). The TI selected should be the time when the signal intensity difference between infarcted and normal myocardial tissue is at its maximum, or immediately after (Fig 14c). If the TI is too short, the signal from normal myocardium will be below the zero crossover point, and the normal myocardial tissue will have a negative magnetization vector at the time of k-space data acquisition (52). Since signal intensity corresponds to the magnitude of the magnetization vector, the signal intensity of normal myocardium increases as the TI becomes shorter, whereas the signal intensity of infarcted myocardial tissue decreases until it reaches the zero crossover point (Fig 14b). At this point, the signal in infarcted myocardium is nulled, and that in normal myocardium is hyperintense. In the opposite extreme, if the TI is too long, the magnetization of normal myocardium will be above zero and the normal tissue will appear gray instead of black. In principle, the optimal TI, at which the signal in normal myocardium is nulled (the so-called null time), must be determined by imaging iteratively with different TI values. To determine the optimal TI, a TI scout sequence may be applied (51). Experienced operators usually can determine the
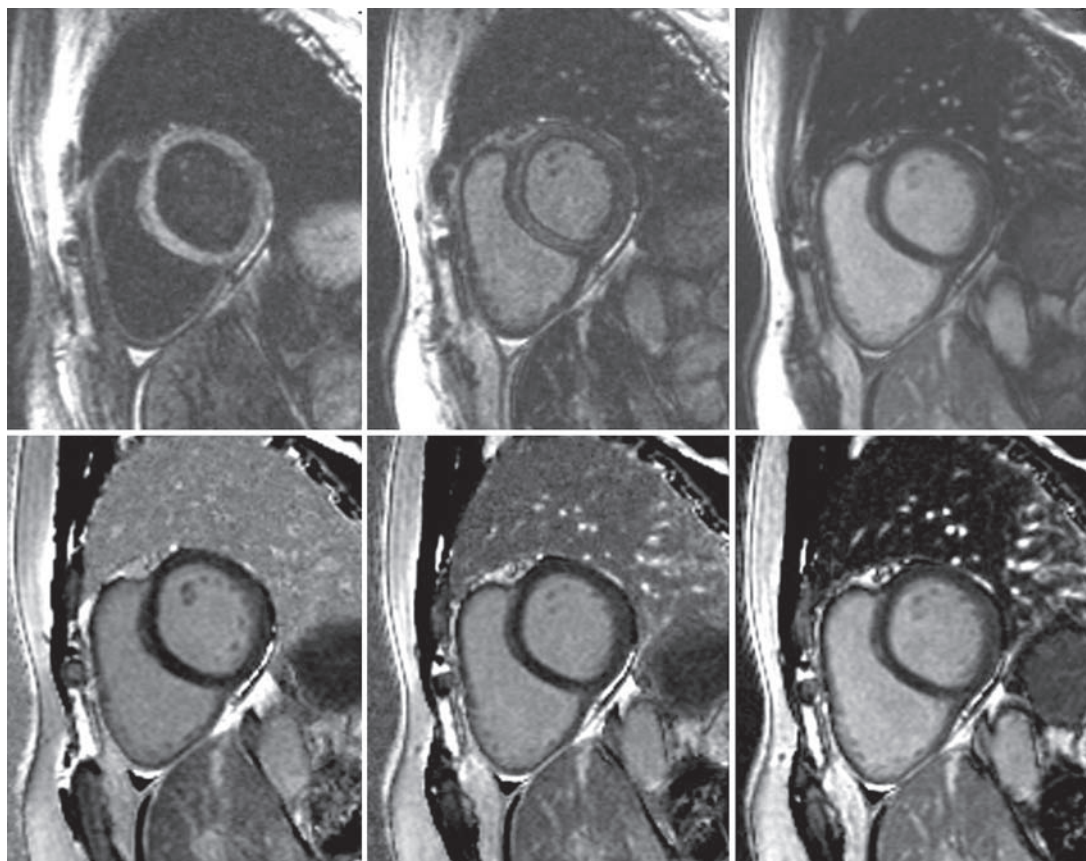
Figure 15.   Magnitude (top row) and phase-sensitive (bottom row) cardiac MR images obtained with a segmented inversion-recovery spoiled GRE sequence in a normal subject with a 3.0-T magnet at TI of 200 msec (left column), 300 msec (middle column), and 350 msec (right column). On the magnitude images, the signal intensity of myocardium is high on the image obtained with the shortest TI (top left); mixed (mottled appearance) on the image obtained with the intermediate TI (top middle); and null on the image obtained with the longest TI (top right). The corresponding phase-sensitive images show relatively null signal in myocardium regardless of TI.

appropriate TI on the basis of one or two such preliminary acquisitions. It is important to keep in mind that the gadolinium concentration within normal myocardium gradually diminishes over time, and the TI must be adjusted upward if delayed enhancement imaging is performed over a long time span (>5 minutes). With conventional magnitude image reconstruction, an error in the null time causes a loss of contrast and polarity artifacts. A phase-sensitive image reconstruction technique may be applied to data acquired with inversion-recovery spoiled GRE or SSFP sequences to maintain contrast and eliminate

polarity artifacts over a relatively wide range of null times (Fig 15) (53,54). This reconstruction technique may be especially useful for radiologists who have little experience in selecting the appropriate TI. However, the TI selected should still be as close as possible to the optimal value to maximize the SNR and contrast-to-noise ratio.

Effects of Suboptimal Delay at Contrast-enhanced Imaging.—Viability imaging is usually performed 10–20 minutes after the intravenous injection of a gadolinium-based contrast material (0.1–0.2 mmol/kg gadolinium) (55). The results of recent studies (9,49,51) suggest that when an appropriate TI is selected, the size of hyperenhanced regions does not change if imaging is per-
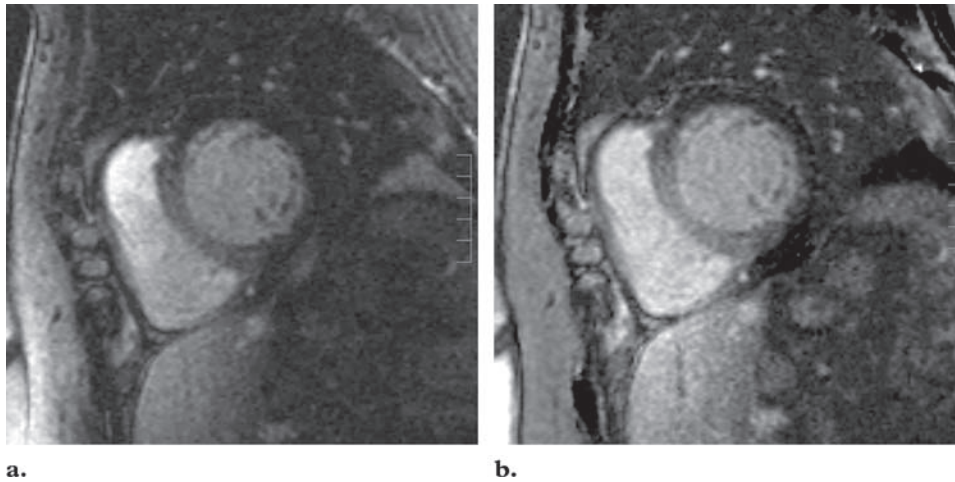
Figure 16. B₁ field inhomogeneity artifact on short-axis delayed cardiac viability images obtained with a 3.0-T MR magnet. Segmented inversion-recovery spoiled GRE magnitude **(a)** and phase **(b)** images show heterogeneous signal suppression in normal myocardium because of inhomogeneity.
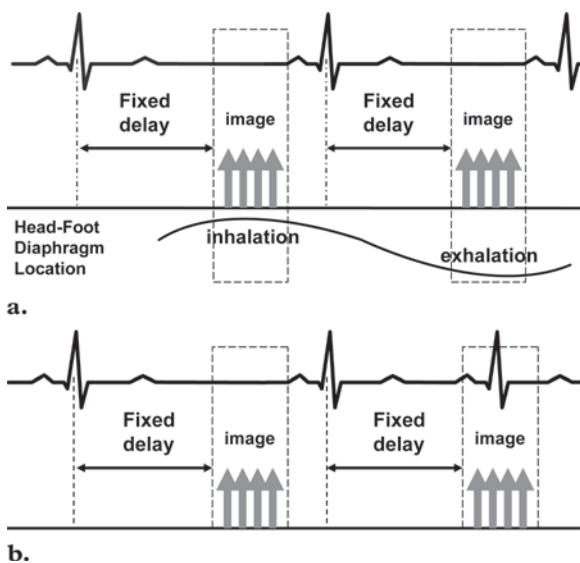

Figure 17. Diagrams show the timing of image acquisition in segmented cardiac MR imaging in relation to breathing **(a)** and ECG gating **(b)** events. Segmented acquisition requires that k-space be filled over several cardiac cycles. In **a,** because of poor breath holding, image acquisition takes place during inhalation and exhalation. In **b,** ectopic beats trigger image acquisition during different parts of the cardiac cycle. (For ease of presentation, **b** shows image acquisition occurring with each heartbeat, although it more commonly is timed to occur with every other heartbeat.)

formed 5–30 minutes after the administration of contrast material. However, it is prudent to wait at least 5 minutes (optimally, 10 minutes) after contrast material administration in order to allow some washout from blood in the left ventricle.

Imaging after a shorter delay, especially when higher initial doses of gadolinium are used, may lead to difficulty in differentiating the signal of the left ventricular cavity from that of the hyperenhanced myocardium.

B₁ Field Inhomogeneity Artifacts.—The use of standard inversion-recovery pulses may result in inhomogeneous signal suppression in normal myocardium and, thus, a false diagnosis of myocardial disease. This phenomenon is especially pronounced at 3.0 T because of the higher B₁ field inhomogeneity of the transmit coils as a result of the interaction of the B₁ field with the body (Fig 16). However, this field inhomogeneity effect often may be reduced by using an adiabatic inversion preparation pulse (56).

Motion-related Ghost Artifacts.—Ghost artifacts due to motion are one of the most common reasons for poor quality of cardiac MR images. Breath holding and ECG gating are usually sufficient to account for these motions during a typical image acquisition time of 8–10 seconds for the two-dimensional version of the segmented inversion-recovery spoiled GRE sequence. Unfortunately, breath holding may be poor and gating inadequate. The segmented nature of the sequence, along with differences in heart position between cardiac cycles, then may lead to motion-induced artifacts (Figs 17, 18).
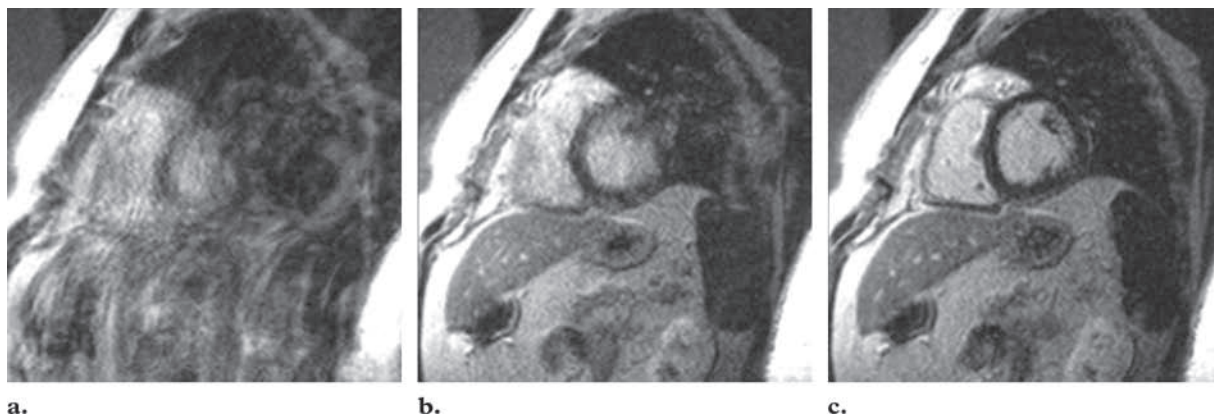
Figure 18.   **(a, b)** Delayed contrast-enhanced MR images show motion-induced ghosts of the heart and chest wall, artifacts of poor breath holding **(a)**, and a ghost of the heart alone **(b)**, an artifact caused by defective ECG gating. **(c)** Delayed contrast-enhanced image obtained with adequate breath holding and ECG gating shows no artifacts.

The image degradation that results from poor ECG gating may be subtle yet sufficient to obscure small subendocardial infarcts or to cause false-positive findings of infarction. Imploring patients to be more careful in breath holding will not lead to an improvement in image quality when the problem is improper cardiac gating. In this regard, it pays to remember that motion artifacts from poor breath holding often cause ghosting (replication) of both the heart and the chest wall, whereas poor ECG gating leads to a ghost or replica of the heart only (Fig 18a, 18b). For some patients, the problem is not an inability to hold the breath for 8–10 seconds, but the fact that "straining" during breath holding leads to small motions that degrade image quality. The solution in this case is to coach the patient to relax during breath holding after normal expiration rather than after forced inspiration or expiration. Likewise, the solution to a cardiac gating problem in a patient with atrial fibrillation or frequent ectopic beats is different from that in a patient with a poor ECG signal. In the latter case, the repositioning of one or more ECG leads may lead to greatly improved image quality.

At imaging in patients who are unable to hold their breath for the duration of the acquisition, a number of approaches are available. Minimizing the FOV in the phase-encoding direction will decrease the number of k-space lines required to complete the image matrix, resulting in faster imaging with no loss in spatial resolution. Occasionally, imaging with only the anterior coil elements (keeping the posterior coils turned off) allows a smaller FOV phase than expected without producing a wraparound artifact over the heart. Another strategy to reduce the breath-hold duration is to increase the number of k-space lines acquired per cardiac cycle, although this results in a reduction in temporal resolution.

In some patients, even with the use of the techniques described earlier, breath holding is inadequate. In this situation, single-shot acquisition techniques may be useful (57). Although there is a reduction in spatial and temporal resolution with single-shot methods, in our experience the inversion recovery–prepared method (single-shot inversion-recovery SSFP) provides reasonable image quality. Compared with the single-shot inversion-recovery spoiled GRE technique, the inversion-recovery SSFP sequence typically allows high-bandwidth imaging (short TE and TR for faster imaging) with good preservation of SNR. Clinical benefits of using this technique are patient comfort, faster imaging, and decrease or elimination of breathing-related artifacts (Fig 19). However, since the inversion-recovery SSFP sequence is typically T2 or T1 weighted, there may be a reduction in the pure T1 contrast effects that normally follow contrast medium adminis-
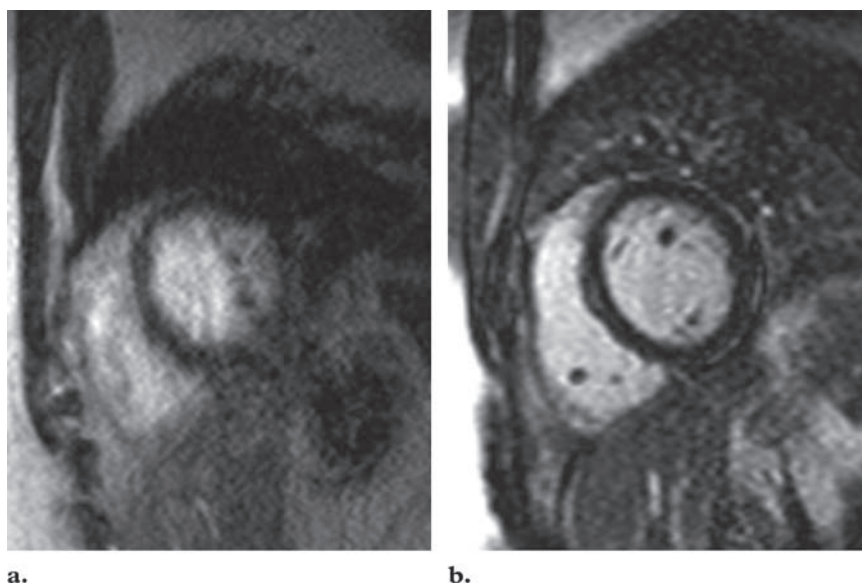
Figure 19. **(a)** Standard segmented inversion-recovery spoiled GRE image obtained in a patient who had difficulty in holding his breath shows a severe respiratory motion–related artifact. **(b)** Short-axis ECG-gated non–breath-hold image from a multisection acquisition obtained with a single-shot inversion-recovery SSFP sequence at the same level as **a** demonstrates a significantly improved appearance.

a.   b.

tration. Single-shot methods also are useful in patients with arrhythmia or with a large amount of pericardial effusion, in whom there may be extensive variations in cardiac position.

We recommend the use of gradient moment nulling, although its deactivation allows the minimum TE and TR to be reduced by 1.0–1.5 msec and enables the use of a lower bandwidth setting (for higher resolution) with the same TR and TE. We make this recommendation because motion-related or flow-induced artifacts may be problematic when gradient moment nulling is turned off, particularly for image acquisitions at the base of the heart. The use of a partial readout gradient as an alternative to gradient moment nulling is an effective means of minimizing the first moment and achieving a minimum TE to reduce T2* effects. The use of a partial readout gradient requires a homodyne reconstruction, a standard technique available on all commercial MR imaging systems (58).

Adjustments of the imaging parameters are often required in patients who have tachycardia or bradycardia. Because of the shorter mid-diastolic period in patients with tachycardia, the number of k-space lines acquired in every cardiac cycle should be reduced to minimize blurring from cardiac motion. In addition, imaging should be

performed during every third heartbeat (gating factor of three) rather than every other heartbeat (gating factor of two) to allow sufficient time for the recovery of magnetization between successive inversion pulses. Incomplete relaxation results in the reduction of the signal intensity difference between infarcted and normal myocardium and may lead to TI shortening with a resultant delay in the nulling of signal in normal myocardium. Because of the latter effect, when the gating factor is increased, the TI to null normal myocardium often must be increased (by 20–40 msec). In patients with bradycardia, triggering with every heartbeat might still allow adequate time for magnetization recovery, while resulting in a 50% reduction in the breath-hold time. Alternatively, or in addition, the number of k-space lines acquired per cardiac cycle may be increased.

Ghost Artifacts from Long T1.—Ghost artifacts also may result from regions within the FOV that have long T1 values (such as cerebrospinal fluid or pericardial effusion). This phenomenon is due to the fact that with long T1, the train of inversion pulses in the segmented inversion-recovery spoiled GRE sequence leads to the

Figure 20. Diagram correlates MR pulse sequence timing (top) with magnetization vectors for various structures (bottom) after administration of an intravenous gadolinium-based contrast material.
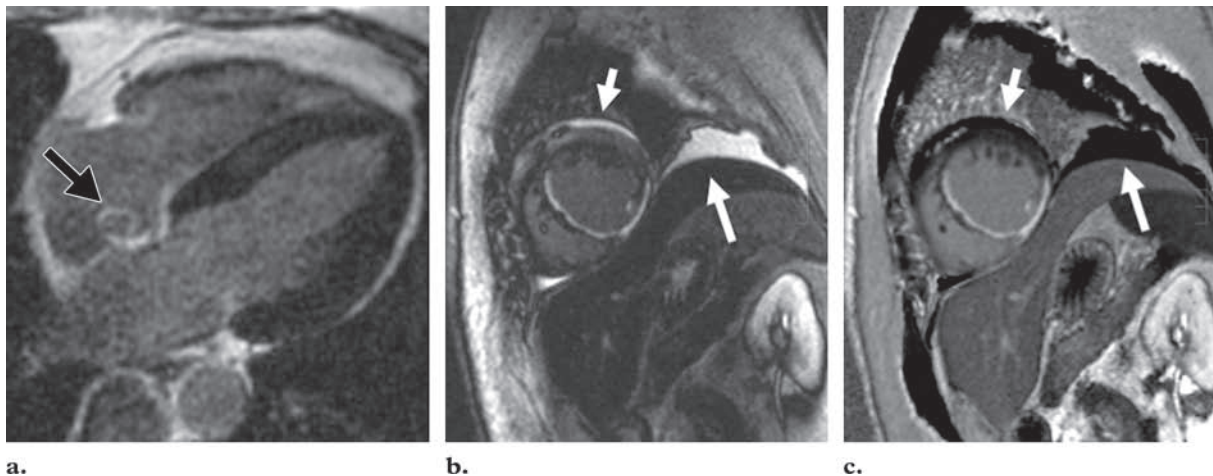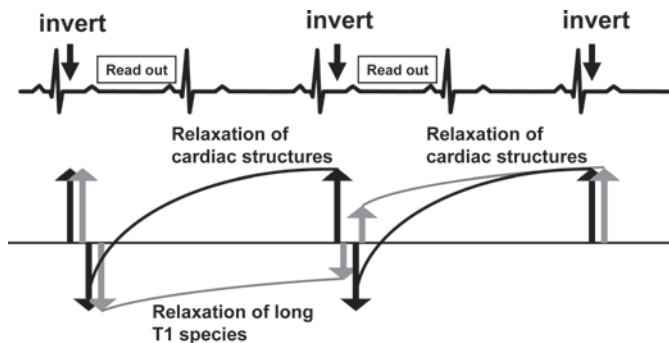

a.   b.   c.

Figure 21. **(a)** Segmented inversion-recovery spoiled GRE image shows a ghost artifact (arrow) due to the long T1 of cerebrospinal fluid. **(b, c)** Short-axis delayed-phase contrast-enhanced images of the heart. Magnitude image **(b)** obtained with the same sequence as used in **a** shows high-signal-intensity pleural and pericardial fluid (arrows), features that are effectively suppressed on the phase image **(c)**. Both images show a large hyperenhancing infarct in the septal and inferior walls of the left ventricle.

oscillation of magnetization before each group of k-space acquisitions (Fig 20). The effect is a ghost artifact that appears in the phase-encoding direction (Fig 21). Ghost artifacts often can be moved outside the region of interest by swapping the frequency-encoding and phase-encoding directions or by using in-plane rotation during image acquisition. However, the applicability of this solution depends on the skill of the operator in immediately identifying the artifact during the image acquisition and on the patient's ability to perform the additional breath holds needed to repeat the acquisition.

For artifacts caused by cerebrospinal fluid and pericardial effusion, a simple solution is to place a saturation slab over the spinal canal or the area of effusion. In a case of pericardial effusion, the

artifact can be reduced by applying a single additional nonselective inversion pulse approximately 2000 msec (the time it takes for the transudate to reach the zero crossover point after the application of an inversion pulse) before the initial 180° inversion pulse of the inversion-recovery sequence. This will result in the suppression of signal from the pericardial effusion (which has a long T1) while maintaining signal in the myocardium (which has a short T1 in the presence of gadolinium). Since such ghost artifacts may be mistaken for myocardial hyperenhancement, the interpreter should be wary of a hyperenhancement pattern that is not in a typical coronary artery distribution. In general, hyperenhanced regions should be verified by acquiring images in at least two orthogonal planes. A fast alternative acquisition method is a phase-sensitive inversion-recovery sequence in which the signal from long
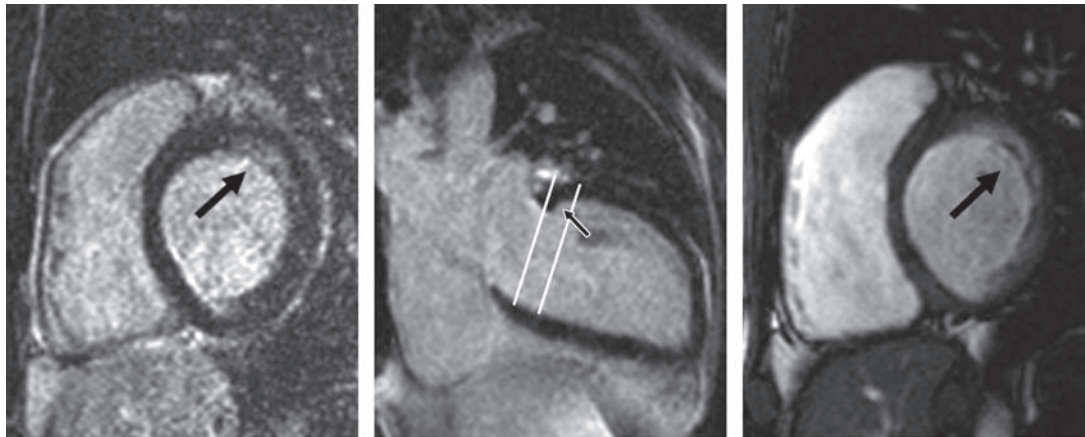
a.   b.   c.

Figure 22.   **(a)** Short-axis delayed contrast-enhanced MR image of the left heart base shows a sub-endocardial high-signal-intensity band along the anterolateral wall of myocardium (arrow), an effect of partial-volume averaging of blood with endocardial trabeculae. **(b)** Long-axis view of the left ventricle shows normal myocardium with a partial-volume averaging effect (arrow) near the base, where the myocardial border is obliquely oriented in relation to the imaging section. **(c)** Short-axis balanced SSFP cine image shows a similar volume averaging artifact (arrow).

T1 species (including cerebrospinal, pleural, and pericardial fluid) is suppressed (Fig 21).

Ghost Artifacts from Short T1 in Fat.—This type of artifact is also common on viability images. The T1 of fat is approximately 250–350 msec. With a heart rate of 75 beats per minute, the R-R interval is 800 msec, which is insufficient time for a short T1 species such as fat to fully recover, and the delay in recovery leads to ghost artifacts. Even small variations in the T1 recovery of fat will lead to significant ghost artifacts, mostly because fat has such high signal intensity. Such artifacts occur exclusively when a single R-R interval is used, and that is the primary reason why at least two R-R intervals should be acquired for viability imaging.

Volume Averaging Artifacts.—Volume averaging effects are most likely to appear along the image axis with the largest voxel diameter. They also occur when structures are oriented obliquely in relation to the imaging plane or when they move in and out of the imaging plane during data acquisition (Fig 22). On short-axis views, volume averaging of epicardial fat with myocardium in regions with abundant epicardial fat, particularly at the cardiac apex and the atrioventricular groove, can lead to apparent hyperenhancement along the epicardial border of the heart. To

determine whether such a feature is artifactual, the acquisition should be repeated with reduced section thickness, a fat suppression technique, or orthogonal views. We do not recommend fat suppression routinely, since high signal intensity in epicardial fat actually may help distinguish between the epicardial border of nulled myocardium and the lung fields, which also have low signal intensity. However, when fat suppression is applied, the k-space lines must be acquired in a centric fashion. With linear acquisition, fat, by virtue of its short T1, will have recovered its signal by the time the central lines of k-space are acquired, negating the attempt at fat suppression.

Velocity-encoded MR Imaging of Flow
A commonly used MR technique to evaluate blood flow is phase-contrast or velocity-encoded MR imaging (59–61). Gradients may be varied in amplitude or duration to sensitize the pulse sequence to fast or slow flow. The operator selects the maximum velocity to be encoded by the sequence. Depending on the sequences available, phase-contrast measurement can be performed in a breath hold or during normal respiration by using prospective or retrospective cardiac gating. Both magnitude and phase images are often reviewed.
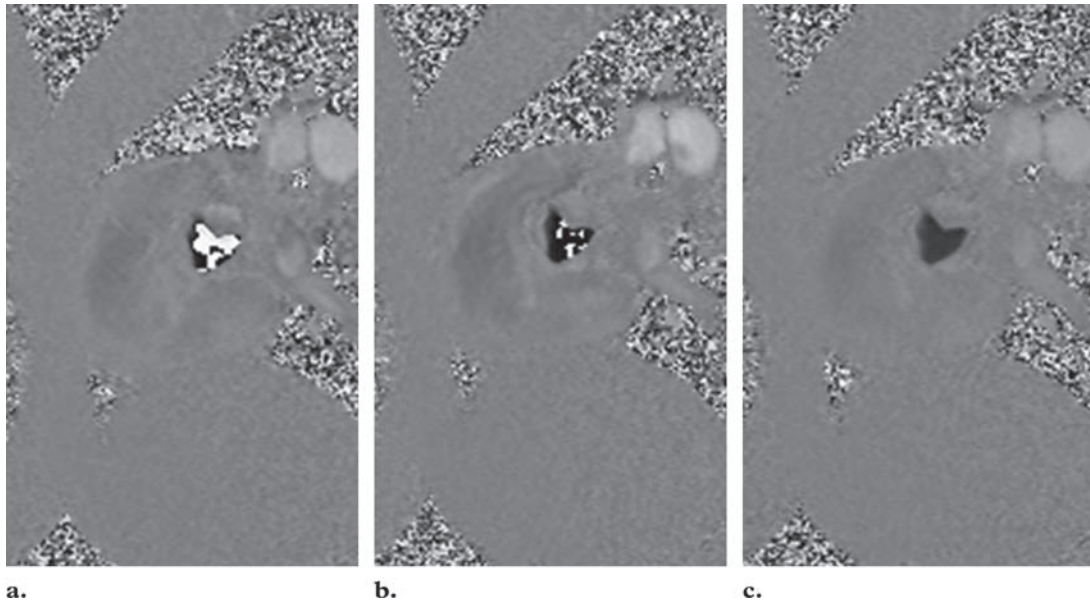
a.   b.   c.

Figure 23.   Adjustment of the velocity encoding threshold for through-plane velocity-encoded imaging of the aortic valve. **(a,b)** Image obtained with a velocity encoding threshold of 150 cm/sec **(a)** shows a severe aliasing artifact (solid white area inside the orifice), an effect that is much diminished when the threshold is increased to 200 cm/sec **(b)**. **(c)** No aliasing is evident when the threshold is increased to 250 cm/sec.

Common errors in phase-contrast imaging are related to inappropriate maximum velocity encoding settings, imaging plane misalignment, partial-volume averaging, inadequate temporal or spatial resolution, and flow and phase offset errors (61).

Aliasing Artifacts.—Aliasing occurs when the maximum velocity sampled exceeds the upper limit imposed by the chosen velocity encoding setting, resulting in apparent velocity reversal. To avoid aliasing, the velocity threshold must be correctly selected. The maximum value selected should slightly exceed the expected velocities.

Aliasing results in an artifactual reduction of the measured flow in direct proportion to the extent (severity) of the aliasing artifact. Fortunately, it is the easiest error to detect in flow measurements. It can be perceived on the velocity images, wherever the voxels of assumed peak velocities have an inverted signal intensity compared with that of surrounding voxels (Fig 23).

Partial-Volume Averaging Effects.—Underestimation of flow and velocity may occur if the voxel selected is too large or if the vessel is not perpendicular to the plane of imaging (62). Too large a voxel size results in reduced measured velocities either because stationary tissues are included in the voxel or because intravoxel dephasing and saturation of slow in-plane flow are increased. Partial-volume averaging artifacts are most commonly seen in small and tortuous vessels. An easy way of decreasing the voxel size (smaller pixels) is to decrease the FOV as much as possible (Fig 24). Remember, a wraparound artifact does not significantly affect the precision of the measurements as long as it is not superposed on the vessel of interest. However, an optimal section thickness is required to achieve optimal SNR. A section thickness of 6–8 mm is optimal to minimize partial-volume averaging effects yet maintain the SNR. For small vessels, section thickness should be reduced to 5 mm. We prefer to obtain velocity measurements after the injection of a gadolinium-based contrast material to improve overall SNR. Often, vessels imaged in
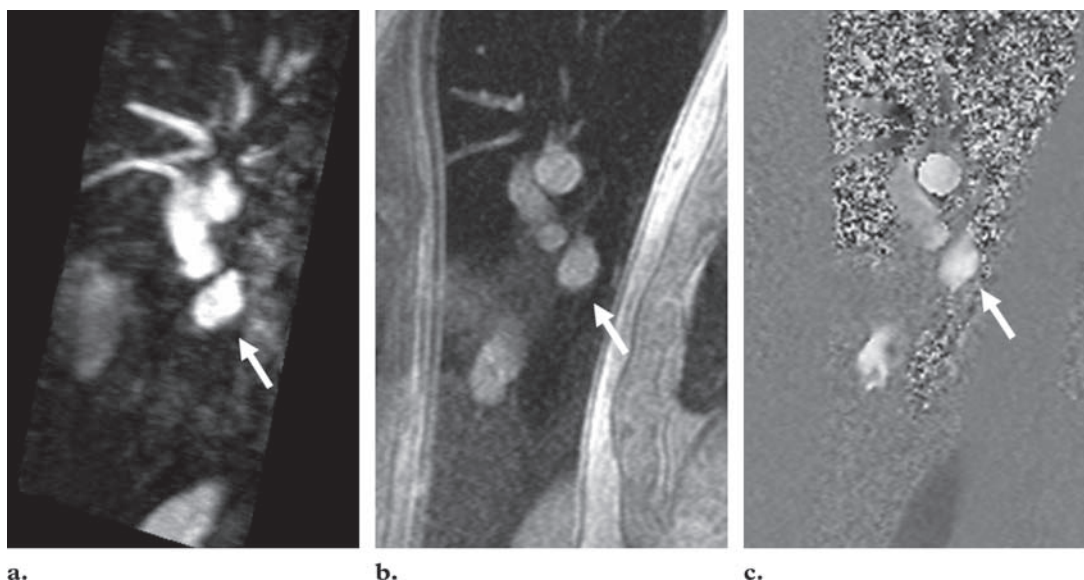
Teaching Point

a.   b.   c.

Figure 24.   **(a)** Cross-sectional image from a three-dimensional MR angiographic data set acquired in a plane perpendicular to the right inferior pulmonary vein (arrow) shows an aliasing artifact. **(b, c)** Magnitude **(b)** and phase **(c)** images, reconstructed with **a** used for localization and with the smallest possible FOV so as to maximize the SNR, show the same artifact. Such artifacts do not significantly affect measurements of flow velocity unless they are superposed on the anatomy of interest.

an orthogonal plane have a circular appearance. However, ovoid contours may be found in veins or vascular prostheses (Fig 24). An ideal orthogonal view of the vessel or a cardiac valve can be obtained from two perpendicular images and be used as a localizing reference to prescribe the appropriate phase-contrast view.

Other Types of Artifacts.—Artifacts from vessel pulsation or cardiac and respiratory motions are common and may interfere with velocity estimates. Unstructured flow (ie, flow with a high Reynolds number) leads to intravoxel dephasing of the signal of flowing spins and causes poor phase-contrast measurements of velocity. This technique is also sensitive to eddy currents, which may occur in the tissue outside the vessel, causing phase shift and incorrect measurements (metal artifacts).

Morphologic Imaging
Pulse sequences currently used for morphologic evaluations can be generally divided into dark-blood and bright-blood techniques. When bright-blood techniques are used, flowing blood has

high signal intensity. Bright-blood techniques are spoiled GRE or balanced SSFP sequences with segmented or single-shot k-space acquisitions. Image contrast when spoiled GRE sequences are used depends on inflow enhancement of blood; when balanced SSFP sequences are used, contrast depends on the steady-state signal of blood, as described earlier. In dark-blood or black-blood imaging techniques, fast-flowing blood appears black or has low signal intensity. Dark-blood techniques eliminate blood flow artifacts unless stagnation is present; therefore, they provide excellent depiction of the architecture of the walls of blood vessels and cardiac chambers. Examples of dark-blood techniques include conventional spin-echo (SE), breath-hold fast SE, single-shot fast SE with double inversion-recovery pulses to suppress the signal from blood (ie, inversion-recovery fast SE), spoiled GRE, and SSFP sequences. The single-shot inversion-recovery fast SE sequence is the most commonly used black-blood technique and can be implemented with
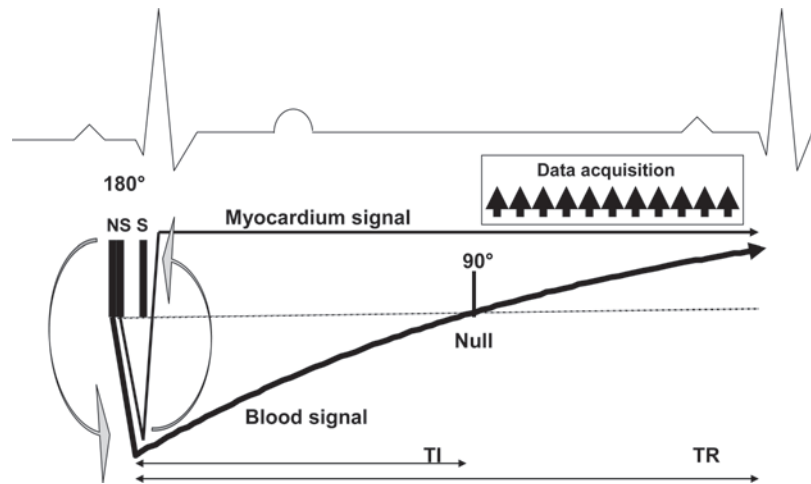
Figure 25.   Diagram of a dark-blood imaging sequence shows the initial inversion of signal from all tissues with the application of a nonselective *(NS)* 180° pulse in late diastole, followed by the restoration of signal in the selected section with the application of a section-selective *(S)* 180° pulse. After a delay *(TI)*, when the signal of flowing blood reaches its null point (in mid diastole), a series of fast SE pulses is applied. The blood signal null point varies with the R-R interval, and TI therefore is shorter in patients with a faster heart rate.
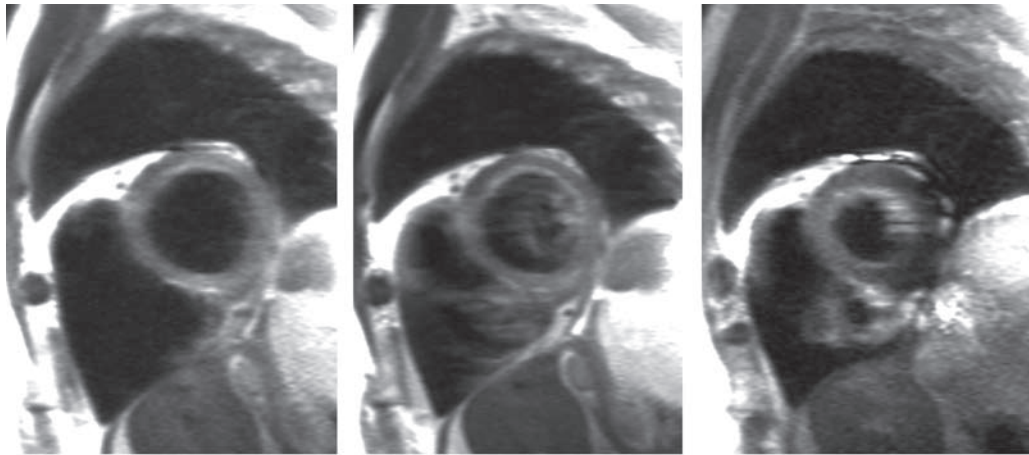

Figure 26.   Short-axis cardiac MR images obtained with a dark-blood inversion-recovery fast SE sequence. **(a)** Image obtained with TR adjusted so that data were acquired in mid diastole provides a clear view of the cardiac chambers. **(b)** Image obtained with too long a TR shows blurring of the chamber walls because of a partial recovery of the signal in blood, an effect that also may be seen on contrast-enhanced images. **(c)** Image obtained with too short a TR shows blurring of the blood-myocardium interface because of base-apex contraction during systole and resultant misalignment of image data from the selective inversion pulse (during diastole) with data from the readout pulses (during systole).
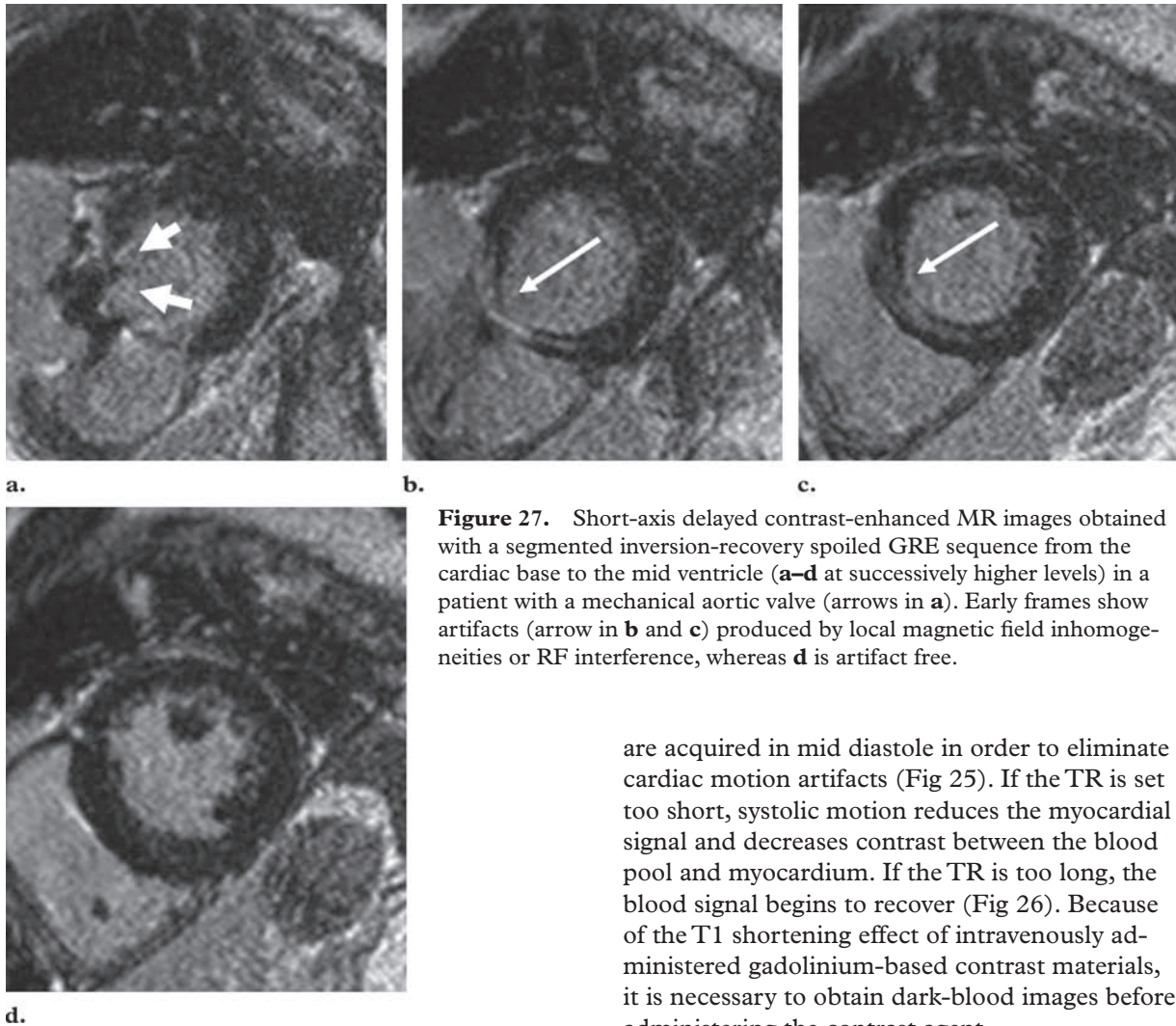
Figure 27.   Short-axis delayed contrast-enhanced MR images obtained with a segmented inversion-recovery spoiled GRE sequence from the cardiac base to the mid ventricle (**a–d** at successively higher levels) in a patient with a mechanical aortic valve (arrows in **a**). Early frames show artifacts (arrow in **b** and **c**) produced by local magnetic field inhomogeneities or RF interference, whereas **d** is artifact free.

or without breath holding (Fig 25) (63). Parallel imaging is performed to improve spatial and temporal resolution in patients with faster heart rates (32). Dark-blood imaging techniques are available in both T1- and T2-weighted variants as well as with and without fat suppression. Note that for T1-weighted variants, the effective TR should be less than 800 msec. For T2-weighted double inversion-recovery sequences, the TR should remain long and the acquisition window should cover two or three heartbeats.

The timing of data acquisition is critical for optimal results. To optimize dark-blood sequences, one should adjust the TR so that data

are acquired in mid diastole in order to eliminate cardiac motion artifacts (Fig 25). If the TR is set too short, systolic motion reduces the myocardial signal and decreases contrast between the blood pool and myocardium. If the TR is too long, the blood signal begins to recover (Fig 26). Because of the T1 shortening effect of intravenously administered gadolinium-based contrast materials, it is necessary to obtain dark-blood images before administering the contrast agent.

Artifacts Caused by Ferromagnetic Materials

Metallic materials are widely used in arterial stents, clips placed during bypass surgery, and prosthetic cardiac valves (64). Artifacts induced by a metallic implant may disrupt the diagnostic capabilities of MR imaging (Fig 27). Generally, two types of metal-induced artifacts may arise: *(a)* magnetic susceptibility artifacts, which arise from local field inhomogeneities caused by the presence of ferromagnetic materials within the magnet, and *(b)* RF artifacts, which are due to
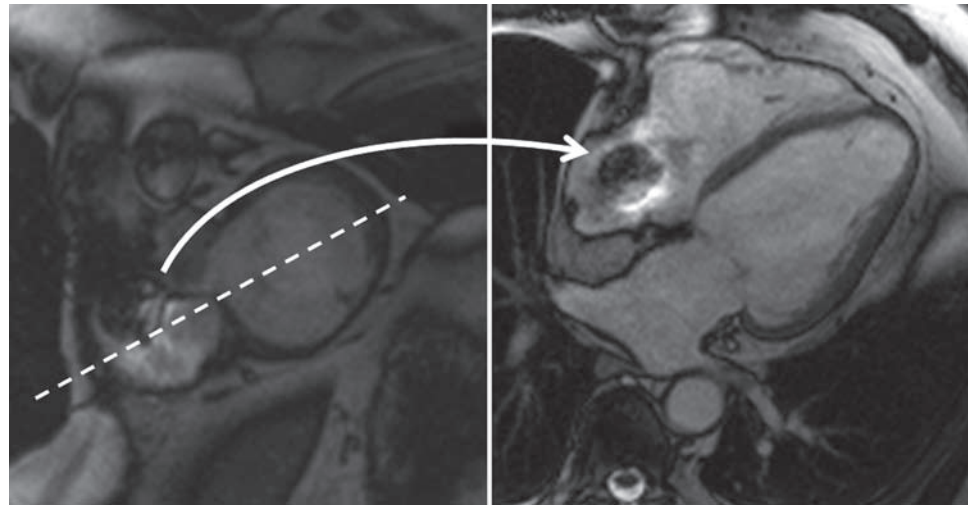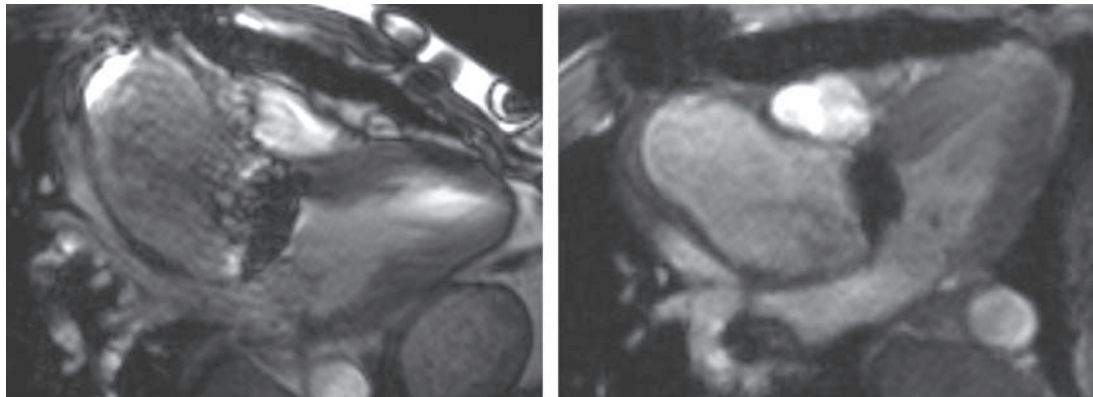
Figure 28.   Short-axis cine images obtained after coronary artery bypass surgery show, near the heart base, large low- and high-signal-intensity artifacts caused by metallic surgical clips placed at the proximal anastomosis to the aorta. The four-chamber view (left) shows a round area that is largely devoid of signal, with a crescentlike rim of higher signal intensity—a typical metal-related artifact—within the right atrium. On the cross-sectional view (right) obtained in the plane indicated (dotted white line), the artifact (curved arrow) might easily be mistaken for a true lesion.

a.   b.

Figure 29.   Long-axis segmented balanced SSFP **(a)** and spoiled GRE **(b)** cine images obtained after an aortic valve replacement show artifacts due to metal-induced local field inhomogeneities, features that are severe in **a** but much less intrusive in **b**.

the deterioration of excitation and refocusing RF pulses caused by the induction of eddy currents in metallic implants (64,65). MR imaging artifacts caused by magnetic susceptibility and RF effects appear as bands with increased or decreased signal intensity around metallic parts (Fig 27). As a result of partial-volume averaging, these artifacts may appear in normal tissue and be mistaken for a pathologic condition (Fig 28).

The severity of susceptibility artifacts in general depends on the pulse sequence used, the magnetic susceptibility of the metal, the orientation of the metallic implant with respect to the

direction of the main magnetic field and the readout direction, the imaging bandwidth, and the strength of the main magnetic field. Magnetic susceptibility leads to two distinct but related artifacts: *(a)* signal loss from T2* decay and *(b)* distortion in the readout direction, particularly at low-frequency bandwidths. RF eddy current artifacts are also dependent on geometry, orientation, and the material of the metallic implant (65,66). In the presence of ferromagnetic materials, magnetic susceptibility artifacts are the major cause of signal loss. With conductive but nonferromagnetic materials such as copper, RF artifacts are more common. Both types of artifacts are more pronounced at 3.0 T.

The artifacts on GRE images differ in appearance from those on SE images. The 180° refocusing pulses in SE sequences compensate for intravoxel dephasing caused by static field inhomogeneities. The influence of TE on the severity of susceptibility artifacts is much greater in GRE imaging than it is in SE imaging. In balanced SSFP imaging, factors that disrupt the steady state, such as magnetic susceptibility variations, result in off-resonance artifacts (Fig 29).

Summary

The continued development of the field of cardiac MR imaging has been paralleled by increased applications. However, each new application (viability and perfusion imaging, cine studies, flow and gradient measurement) is vulnerable to artifacts that may undermine the diagnostic value of the images. Knowledge about the causes and appearances of these artifacts is essential in order to avoid misinterpreting them as true lesions. In addition, those who perform cardiac MR imaging studies should be familiar with the available methods for eliminating artifacts or at least lessening their severity.

References

1. Sakuma H, Fujita N, Foo TK, et al. Evaluation of left ventricular volume and mass with breath-hold cine MR imaging. Radiology 1993;188:377–380.
2. Lanzer P, Barta C, Botvinick EH, Wiesendanger HU, Modin G, Higgins CB. ECG-synchronized cardiac MR imaging: method and evaluation. Radiology 1985;155:681–686.
3. Barkhausen J, Ruehm SG, Goyen M, et al. MR evaluation of ventricular function: true fast imaging with steady-state precession versus fast low-angle shot cine MR imaging: feasibility study. Radiology 2001;219:264–269.
4. Atkinson DJ, Edelman R. Cineangiography of the heart in a single breath hold with a segmented TurboFLASH sequence. Radiology 1991;178:357–360.
5. Carr JC, Simonetti O, Bundy J, Li D, Pereles S, Finn JP. Cine MR angiography of the heart with segmented true fast imaging with steady-state precession. Radiology 2001;219:828–834.
6. Atkinson DJ, Burstein D, Edelman RR. First-pass cardiac perfusion: evaluation with ultrafast MR imaging. Radiology 1990;174:757–762.
7. Reeder SB, Atalar E, Faranesh AZ, McVeigh ER. Multi-echo segmented k-space imaging: an optimized hybrid sequence for ultrafast cardiac imaging. Magn Reson Med 1999;41(2):375–385.
8. Epstein FH, Wolff SD, Arai AE. Segmented k-space fast cardiac imaging using an echo-train readout. Magn Reson Med 1999;41(3):609–661.
9. Kim RJ, Wu E, Rafael A, et al. The use of contrast-enhanced magnetic resonance imaging to identify reversible myocardial dysfunction. N Engl J Med 2000;343:1445–1453.
10. Wood ML, Henkelman RM. Artifacts. In: Stark DD, Bradley WG Jr, eds. Magnetic resonance imaging. St. Louis, Mo: Mosby, 1999; 215–230.
11. Taylor AM, Jhooti P, Wiesmann F, Keegan J, Firmin DN, Pennell DJ. MR navigator-echo monitoring of temporal changes in diaphragm position: implications for MR coronary angiography. J Magn Reson Imaging 1997;7(4):629–636.
12. Fischer SE, Wickline SA, Lorenz CH. Novel real-time R-wave detection algorithm based on the vectorcardiogram for accurate gated magnetic resonance acquisitions. Magn Reson Med 1999;42(2):361–370.
13. Hennig J. Generalized MR interferography. Magn Reson Med 1990;16:390–402.
14. Zhuo J, Gullapalli RP. AAPM/RSNA physics tutorial for residents: MR artifacts, safety, and quality control. RadioGraphics 2006;26(1):275–297.
15. Lee VS, Resnick D, Bundy JM, Simonetti OP, Lee P, Weinreb JC. Cardiac function: MR evaluation in one breath hold with real-time true fast imaging with steady-state precession. Radiology 2002;222:835–842.
16. Barkhausen J, Goyen M, Rühm SG, Eggebrecht H, Debatin JF, Ladd ME. Assessment of ventricular function with single breath-hold real-time steady-state free precession cine MR imaging. AJR Am J Roentgenol 2002;178:731–735.

17. Miller S, Simonetti OP, Carr J, Kramer U, Finn JP. MR imaging of the heart with cine true fast imaging with steady-state precession: influence of spatial and temporal resolutions on left ventricular functional parameters. Radiology 2002;223:263–269.

18. Spuentrup E, Schroeder J, Mahnken AH, et al. Quantitative assessment of left ventricular function with interactive real-time spiral and radial MR imaging. Radiology 2003;227:870–876.

19. Scheffler K, Lehnhardt S. Principles and applications of balanced SSFP techniques. Eur Radiol 2003;13(11):2409–2418.

20. Nayak KS, Hargreaves BA, Hu BS, Nishimura DG, Pauly JM, Meyer CH. Spiral balanced steady-state free precession cardiac imaging. Magn Reson Med 2005;53(6):1468–1473.

21. Reeder SB, Faranesh AZ, Boxerman JL, McVeigh ER. In vivo measurement of T*2 and field inhomogeneity maps in the human heart at 1.5 T. Magn Reson Med 1998;39(6):988–998.

22. Atalay MK, Poncelet BP, Kantor HL, Brady TJ, Weisskoff RM. Cardiac susceptibility artifacts arising from the heart-lung interface. Magn Reson Med 2001;45(2):341–345.

23. Markl M, Alley M, Elkins C, Pelc N. Flow effects in balanced steady state free precession imaging. Magn Reson Med 2003;50:892–903.

24. Li W, Storey P, Chen Q, Li BS, Prasad PV, Edelman RR. Dark flow artifacts with steady-state free precession cine MR technique: causes and implications for cardiac MR imaging. Radiology 2004; 230:569–575.

25. Wansapura J, Fleck R, Crotty E, Gottliebson W. Frequency scouting for cardiac imaging with SSFP at 3 Tesla. Pediatr Radiol 2006;36(10):1082–1085.

26. Sodickson DK, Manning WJ. Simultaneous acquisition of spatial harmonics (SMASH): fast imaging with radiofrequency coil arrays. Magn Reson Med 1997;38:591–603.

27. Pruessmann KP, Weiger M, Scheidegger MB, et al. SENSE: sensitivity encoding for fast MRI. Magn Reson Med 1999;42:952–962.

28. Griswold MA, Jakob PM, Heidemann RM, et al. Generalized autocalibrating partially parallel acquisitions (GRAPPA). Magn Reson Med 2002;47: 1202–1210.

29. Griswold MA, Kannengiesser S, Heidemann RM, Wang J, Jakob PM. Field-of-view limitations in parallel imaging. Magn Reson Med 2004;52(5): 1118–1126.

30. Sodickson DK, McKenzie CA. A generalized approach to parallel magnetic resonance imaging. Med Phys 2001;28:1629–1643.

31. Hinton DP, Wald LL, Pitts J, et al. Comparison of cardiac MRI on 1.5 and 3.0 Tesla clinical whole body systems. Invest Radiol 2003;38:436–442.

32. Greenman RL, Shirosky JE, Mulkern RV, et al. Double inversion black-blood fast spin-echo imaging of the human heart: a comparison between 1.5 T and 3.0 T. J Magn Reson Imaging 2003;17: 648–655.

33. McGee KP, Debbins JP, Boskamp EB, Blawat L, Angelos L, King KF. Cardiac magnetic resonance parallel imaging at 3.0 Tesla: technical feasibility and advantages. J Magn Reson Imaging 2004; 19(3):291–297.

34. Goldfarb JW. The SENSE ghost: field-of-view restrictions for SENSE imaging. J Magn Reson Imaging 2004;20(6):1046–1051.

35. Park J, Zhang Q, Jellus V, Simonetti O, Li D. Artifact and noise suppression in GRAPPA imaging using improved k-space coil calibration and variable density sampling. Magn Reson Med 2005; 53(1):186–193.

36. Kellman P, Epstein FH, McVeigh ER. Adaptive sensitivity encoding incorporating temporal filtering (TSENSE). Magn Reson Med 2001;45: 846–852.

37. Madore B, Glover GH, Pelc NJ. Unaliasing by Fourier-encoding the overlaps using the temporal dimension (UNFOLD), applied to cardiac imaging and fMRI. Magn Reson Med 1999;42:813–828.

38. Breuer FA, Kellman P, Griswold MA, Jakob PM. Dynamic autocalibrated parallel imaging using temporal GRAPPA (TGRAPPA). Magn Reson Med 2005;53(4):981–985.

39. Epstein FH, London JF, Peters DC, et al. Multislice first-pass cardiac perfusion MRI: validation in a model of myocardial infarction. Magn Reson Med 2002;47:482–491.

40. Schreiber WG, Schmitt M, Kalden P, Mohrs OK, Kreitner KF, Thelen M. Dynamic contrast-enhanced myocardial perfusion imaging using saturation-prepared TrueFISP. J Magn Reson Imaging 2002;16:641–652.

41. Wang Y, Moin K, Akinboboye O, Reichek N. Myocardial first pass perfusion: steady-state free precession versus spoiled gradient echo and segmented echo planar imaging. Magn Reson Med 2005;54: 1123–1129.

42. Storey P, Chen Q, Li W, Edelman RR, Prasad PV. Band artifacts due to bulk motion. Magn Reson Med 2002;48:1028–1036.

43. Barkhausen J, Hunold P, Jochims M, Debatin JF. Imaging of myocardial perfusion with magnetic resonance. J Magn Reson Imaging 2004;19: 750–757.

44. Di Bella EV, Parker DL, Sinusas AJ. On the dark rim artifact in dynamic contrast-enhanced MRI myocardial perfusion studies. Magn Reson Med 2005;54:1295–1299.

45. Glockner JF, Hu HH, Stanley DW, Angelos L, King K. Parallel MR imaging: a user's guide. RadioGraphics 2005;25:1279–1297.

46. Neimatallah MA, Chenevert TL, Carlos RC, et al. Subclavian MR arteriography: reduction of susceptibility artifact with short echo time and dilute gadopentetate dimeglumine. Radiology 2000;217: 581–586.

47. Ba-Ssalamah A, Nobauer-Huhmann IM, Pinker K, et al. Effect of contrast dose and field strength in the magnetic resonance detection of brain metastases. Invest Radiol 2003;38(7):415–422.

48. Wu KC, Zerhouni EA, Judd RM, et al. Prognostic significance of microvascular obstruction by magnetic resonance imaging in patients with acute myocardial infarction. Circulation 1998;97(8): 765–772.

49. Lima JA, Judd RM, Bazille A, Schulman SP, Atalar E, Zerhouni EA. Regional heterogeneity of human myocardial infarcts demonstrated by contrast-enhanced MRI. Potential mechanisms. Circulation 1995;92(5):1117–1125.

50. Rochitte CE, Lima JA, Bluemke DA, et al. Magnitude and time course of microvascular obstruction and tissue injury after acute myocardial infarction. Circulation 1998;98(10):1006–1014.

51. Simonetti OP, Kim RJ, Fieno DS, et al. An improved MR imaging technique for the visualization of myocardial infarction. Radiology 2001;218: 215–223.

52. Kim RJ, Shah DJ, Judd RM. How we perform delayed enhancement imaging. J Cardiovasc Magn Reson 2003;5:505–514.

53. Kellman P, Arai AE, McVeigh ER, Aletras AH. Phase sensitive inversion recovery for detecting myocardial infarction using gadolinium-delayed hyperenhancement. Magn Reson Med 2002;47: 372–383.

54. Huber AM, Schoenberg SO, Hayes C, et al. Phase-sensitive inversion-recovery MR imaging in the detection of myocardial infarction. Radiology 2005; 237(3):854–860.

55. Mahrholdt H, Wagner A, Holly TA, et al. Reproducibility of chronic infarct size measurement by contrast-enhanced magnetic resonance imaging. Circulation 2002;106:2322–2327.

56. Gutberlet M, Noeske R, Schwinge K, Freyhardt P, Felix R, Niendorf T. Comprehensive cardiac magnetic resonance imaging at 3.0 Tesla: feasibility and implications for clinical applications. Invest Radiol 2006;41(2):154–167.

57. Huber A, Schoenberg SO, Spannagl B, et al. Single-shot inversion recovery TrueFISP for assessment of myocardial infarction. AJR Am J Roentgenol 2006;186(3):627–633.

58. Noll DC, Nishimura DG, Macovski A. Homodyne detection in magnetic resonance imaging. IEEE Trans Med Imaging 1991;10:154–163.

59. Underwood SR, Firmin DN, Klipstein RH, Rees RS, Longmore DB. Magnetic resonance velocity mapping: clinical application of a new technique. Br Heart J 1987;57:404–412.

60. Spritzer CE, Pelc NJ, Lee JN, Evans AJ, Sostman HD, Riederer SJ. Rapid MR imaging of blood flow with a phase-sensitive, limited-flip-angle, gradient recalled pulse sequence: preliminary experience. Radiology 1990;176:255–262.

61. Lotz J, Meier C, Leppert A, Galanski M. Cardiovascular flow measurement with phase-contrast MR imaging: basic facts and implementation. RadioGraphics 2002;22:651–671.

62. Tang C, Blatter DD, Parker DL. Accuracy of phase contrast flow measurements in the presence of partial-volume effects. J Magn Reson Imaging 1993;3: 377–385.

63. Simonetti OP, Finn JP, White RD, Laub G, Henry DA. "Black blood" T2-weighted inversion-recovery MR imaging of the heart. Radiology 1996;199(1): 49–57.

64. Edwards MB, Taylor KM, Shellock FG. Prosthetic heart valves: evaluation of magnetic field interactions, heating, and artifacts at 1.5 Tesla. J Magn Reson Imaging 2000;12:363–369.

65. Bartels LW, Smits HF, Bakker CJ, Viergever MA. MR imaging of vascular stents: effects of susceptibility, flow, and radiofrequency eddy currents. J Vasc Interv Radiol 2001;12:365–371.

66. Camacho CR, Plewes DB, Henkelman RM. Non-susceptibility artifacts due to metallic objects in MR imaging. J Magn Reson Imaging 1995;5: 75–88.

RadioGraphics

Optimizing Cardiac MR Imaging: Practical Remedies for Artifacts

Farhood Saremi, MD, et al

Page 1168
Because dark band artifacts are related to inhomogeneities in the magnetic field or center frequency offsets, they may be substantially reduced by reshimming and retuning of the imaging system.

Page 1168
Parallel imaging methods may help accelerate image acquisition, but at the costs of reduced SNR and increased artifacts.

Page 1171
Dark subendocardial rim artifacts are common in perfusion studies and may be confused with myocardial perfusion defects.

Page 1173
Selecting the appropriate TI is extremely important for obtaining accurate images.

Page 1180
Aliasing results in an artifactual reduction of the measured flow in direct proportion to the extent (severity) of the aliasing artifact.